

# Fair CCA for Fair Representation Learning: An ADNI Study

Bojian Hou\*  
bojianh@upenn.edu  
University of Pennsylvania  
Philadelphia, Pennsylvania, USA

Zhanliang Wang\*  
zhanliang.wang@pennmedicine.upenn.edu  
University of Pennsylvania  
Philadelphia, Pennsylvania, USA

Zhuoping Zhou  
zhuopinz@sas.upenn.edu  
University of Pennsylvania  
Philadelphia, Pennsylvania, USA

Boning Tong  
boningt@seas.upenn.edu  
University of Pennsylvania  
Philadelphia, Pennsylvania, USA

Zexuan Wang  
zxwang@sas.upenn.edu  
University of Pennsylvania  
Philadelphia, Pennsylvania, USA

Jingxuan Bao  
bao96@sas.upenn.edu  
University of Pennsylvania  
Philadelphia, Pennsylvania, USA

Duy Duong-Tran<sup>†</sup>  
dduongtr@upenn.edu  
University of Pennsylvania  
Philadelphia, Pennsylvania, USA

Qi Long  
tywei@alumni.upenn.edu  
University of Pennsylvania  
Philadelphia, Pennsylvania, USA

Li Shen<sup>‡</sup>  
li.shen@pennmedicine.upenn.edu  
University of Pennsylvania  
Philadelphia, Pennsylvania, USA

## Abstract

Canonical correlation analysis (CCA) is a technique for finding correlations between different data modalities and learning low-dimensional representations. As fairness becomes crucial in machine learning, fair CCA has gained attention. However, previous approaches often overlook the impact on downstream classification tasks, limiting applicability. We propose a novel fair CCA method for fair representation learning, ensuring the projected features are independent of sensitive attributes, thus enhancing fairness without compromising accuracy. We validate our method on synthetic data and real-world data from the Alzheimer’s Disease Neuroimaging Initiative (ADNI), demonstrating its ability to maintain high correlation analysis performance while improving fairness in classification tasks. Our work enables fair machine learning in neuroimaging studies where unbiased analysis is essential.

## CCS Concepts

• Computing methodologies → Machine learning algorithms;

## Keywords

CCA, Fairness, Representation Learning, Alzheimer’s Disease

## 1 Introduction

Canonical correlation analysis (CCA) is a well-established technique for exploring the relationship between two sets of multi-dimensional variables. By finding a pair of linear transformations that maximize the correlation between the projected variables, CCA enables the discovery of latent factors that capture the shared information across different modalities [15]. CCA’s ability to preserve cross-modal correlations has made it widely used in biology [31], neuroscience [2] to medicine [44], and engineering [8].

Despite widespread adoption, conventional CCA methods do not account for potential biases concerning sensitive attributes such as sex, race, or age. This lack of fairness consideration can lead to learned representations that capture and amplify undesirable

societal biases, resulting in discriminatory outcomes in downstream applications [5, 34]. As machine learning models are increasingly deployed in high-stakes decision-making scenarios, it is imperative to develop fair representation learning techniques that mitigate these biases while preserving the utility of the learned features [42].

A recent study [45] developed fair CCA methods that minimize correlation disparity errors associated with protected attributes, ensuring equitable correlation levels across different groups. The authors proposed a single-objective fair CCA (SF-CCA) and a multi-objective fair CCA (MF-CCA). SF-CCA is more efficient with a fixed set of hyperparameters, while MF-CCA can automatically identify the optimal hyperparameters. However, these fair CCA methods primarily focus on correlation analysis without explicitly considering the subsequent classification or prediction tasks that often motivate using CCA. Such disconnection between the state-of-the-art CCA learnings and the downstream tasks could significantly hinder the broader applicability of fair CCA. Furthermore, although MF-CCA has the advantage of automatic hyperparameter tuning, its complex optimization techniques limit its efficiency, which, in turns, prevent its wider adoption in application domain.

In this paper, we introduce a novel fair CCA method that implicitly optimizes for both fairness and classification performance. Our approach enforces independence between the learned representations and sensitive attributes, thereby promoting fairness. By utilizing CCA, we maintain high correlation between multimodal data, which facilitates improved performance in subsequent classification tasks.

Specifically, as illustrated in Figure 1, panels (a)–(c) showcase the general framework of CCA. Two samples  $\mathbf{x}_1$  and  $\mathbf{x}_2$  from the first data matrix  $\mathbf{X}$ , and  $\mathbf{y}_1$  and  $\mathbf{y}_2$  from the second data matrix  $\mathbf{Y}$  are projected into the same feature space. This projection aims to maximize correlations between corresponding samples, which are inversely related to the angles between the sample vectors  $\mathbf{x}_i$  and  $\mathbf{y}_i$  ( $i = 1$  or  $2$ ). Panels (d)–(g) compare the results of different learning strategies. Four pairs of samples are shown, with female pairs highlighted in red and male pairs in blue. Sex-based projection matrices heavily bias the final projection, favoring one sex over the other (panels (d) and (e)). While CCA reduces angles compared to random

<sup>\*</sup>Equal contributions

<sup>†</sup>Also affiliated with The United States Naval Academy, Annapolis, Maryland, USA

<sup>‡</sup>Corresponding author

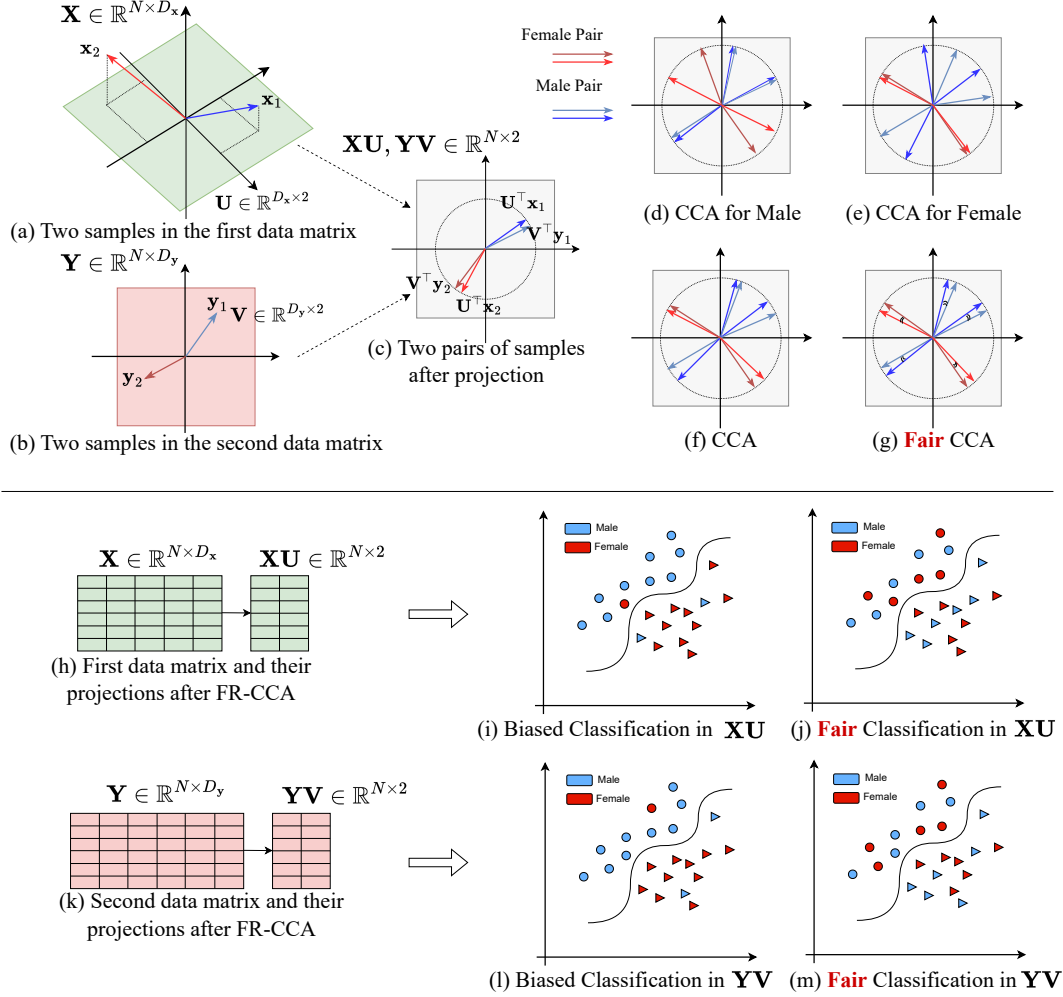


**Figure 1: Illustration of FR-CCA with the sensitive attribute sex as an example (female and male). (a)–(c) demonstrate the general framework of CCA, while (d)–(g) provide a comparison of the projected results using various strategies. It is important to note that the correlation between two corresponding samples is inversely associated with the angle formed by their projected vectors. FR-CCA aims to equalize the average angles among different groups. After projection ((h) and (k)), our FR-CCA can lead to fair classification ((j) and (m)), where the classification results will not be affected by the sex information.**

projection (panel (f)), significant angle differences between male and female pairs indicate persistent bias. Our proposed FR-CCA addresses this bias by maximizing correlation within pairs while ensuring equal correlations across different groups, such as males and females (panel (g)). Panels (h) and (k) illustrate the original data matrices  $\mathbf{X}$  and  $\mathbf{Y}$  and their projections after FR-CCA,  $\mathbf{XU}$  and  $\mathbf{YV}$ , respectively. Panels (i) and (j) demonstrate biased and fair classification on  $\mathbf{XU}$  before and after FR-CCA. The biased classification significantly relies on sex information, while fair classification shows more balanced sex representation in each class. Similar results are shown in panels (l) and (m) for  $\mathbf{YV}$  before and after FR-CCA.

We evaluate the proposed fair CCA method on various datasets, including synthetic and real datasets, with a particular focus on Alzheimer’s disease (AD) diagnosis. In the clinical context of AD, ensuring fairness is crucial due to the demographic diversity of

the patient population and the high stakes of diagnostic decisions. Traditional diagnostic models may inadvertently incorporate biases related to age, sex, or race, potentially leading to unequal access to diagnosis and treatment options.

Applying our fair CCA method to AD diagnosis involves leveraging multimodal data, such as PET and MRI imaging information, to uncover latent factors critical for accurate diagnosis. By ensuring that these latent factors are unbiased regarding sensitive attributes, our method helps develop equitable diagnostic tools that are equitable across different demographic groups. This fairness aspect is particularly important in clinical settings, where biased diagnostic outcomes can significantly affect implications for patient care and treatment strategies [30].

Our empirical results demonstrate that the proposed method achieves superior fairness-accuracy trade-offs compared to existing

fair CCA techniques. In the clinical context of AD, this means more accurate and equitable diagnosis across diverse patient groups, enhancing the reliability and inclusiveness of diagnostic tools. By addressing both fairness and performance, our method offers a practical solution for fair representation learning in real-world scenarios, particularly in high-stakes fields like medicine, where equitable treatment is paramount.

## 2 Related Work

**Canonical Correlation Analysis (CCA)**, introduced by Hotelling in 1936 [14], has been widely applied across various domains. In the context of representation learning, particularly for cross-modal applications, Deep CCA [3] extended traditional CCA to learn nonlinear transformations of two views of data, enabling the discovery of complex correlations in high-dimensional spaces. This advancement has been particularly relevant in fields such as neuroscience [2] and medicine [44], where multimodal data analysis [29] is crucial. Recent work has also explored probabilistic formulations of CCA [4], further expanding its utility in domains like bioinformatics and computer vision.

**Fairness in Machine Learning** As machine learning models are increasingly deployed in high-stakes decision-making scenarios, ensuring fairness has become a critical concern. Seminal work by Dwork et al. (2012) [11] introduced the concept of individual fairness, while subsequent research has explored various group fairness metrics and their implications [5, 16, 34]. In the context of representation learning, Zemel et al. (2013) [42] proposed methods for learning fair representations independent of protected attributes. This line of research is particularly relevant to our work, as we aim to develop fair CCA methods that mitigate biases while preserving the utility of learned features.

**Fair CCA** Recent efforts have focused on incorporating fairness considerations directly into the CCA framework. Zhou et al. (2024) [45] developed fair CCA methods that minimize correlation disparity errors associated with protected attributes. Their work introduced single-objective fair CCA (SF-CCA) and multi-objective fair CCA (MF-CCA), to ensure equitable correlation levels across different groups. However, these methods primarily focus on the correlation analysis without explicitly considering for downstream tasks. Our work builds upon these foundations, addressing the limitations by jointly optimizing for fairness and classification performance.

**Machine Learning for Alzheimer’s Disease (AD)** The application of machine learning to Alzheimer’s Disease diagnosis has seen significant advancements in recent years. Multimodal approaches integrating neuroimaging, genetic, and clinical data have enhanced predictive performance [37–39, 43]. In the context of fair machine learning, recent work has highlighted the importance of developing unbiased diagnostic tools that perform equitably across diverse patient groups [30]. Our research contributes to this area by applying fair CCA methods to AD diagnosis, leveraging multimodal data such as PET and MRI imaging information to uncover latent factors that are both critical for accurate diagnosis and unbiased with respect to sensitive attributes.

A more comprehensive related work can be found in Appendix C.

## 3 Preliminaries

CCA is a multivariate statistical technique that explores the relationship between two sets of variables [15]. Given two datasets  $\mathbf{X} \in \mathbb{R}^{N \times D_x}$  and  $\mathbf{Y} \in \mathbb{R}^{N \times D_y}$  on the same set of  $N$  observations, CCA seeks the  $R$ -dimensional subspaces where the projections of  $\mathbf{X}$  and  $\mathbf{Y}$  are maximally correlated. In other words, CCA finds  $\mathbf{U} \in \mathbb{R}^{D_x \times R}$  and  $\mathbf{V} \in \mathbb{R}^{D_y \times R}$  such that

$$\begin{aligned} \max \quad & \text{trace}(\mathbf{U}^\top \mathbf{X}^\top \mathbf{Y} \mathbf{V}) \\ \text{subject to} \quad & \mathbf{U}^\top \mathbf{X}^\top \mathbf{X} \mathbf{U} = \mathbf{V}^\top \mathbf{Y}^\top \mathbf{Y} \mathbf{V} = \mathbf{I}_R. \end{aligned} \quad (\text{CCA})$$

Next, we review some notions of fairness in the classification task.

**DEFINITION 1.** Let  $f$  be a score function that maps the random variable  $X$  to a real number.

- **Demographic Parity (DP):**  $f$  satisfies demographic parity with respect to  $A$  if  $\mathbb{E}[f(X)] = \mathbb{E}[f(X)|A]$ .
- **Equalized Odds (EO):**  $f$  satisfies equalized odds with respect to  $A$  if  $\mathbb{E}[f(X)|Y] = \mathbb{E}[f(X)|Y, A]$ .
- **Group Sufficiency (GS):**  $f$  is sufficient with respect to attribute  $A$  if  $\mathbb{E}[Y|f(X)] = \mathbb{E}[Y|f(X), A]$ .

DP ensures that the expected score  $f(X)$  remains constant, regardless of the attribute  $A$ . This principle guarantees that the distribution of scores remains unaffected by the sensitive attribute, thereby promoting fairness in the decision-making process. EO dictates that the expected score  $f(X)$  remains consistent across all combinations of labels  $Y$  and attributes  $A$ . It ensures that individuals sharing the same label but differing attributes are treated equally in terms of their predicted scores, irrespective of the sensitive attribute. GS ensures the score function  $f$  captures all the information about the label  $Y$  that is relevant for prediction, regardless of the attribute  $A$ . Definition 1 leads to a notion of the *demographic parity gap* (DPG), *equalized odds gap* (EOG), and *group sufficiency gap* (GSG) defined, respectively, as:

$$\text{DPG}_f(A) = \mathbb{E}[\mathbb{E}[f(X)] - \mathbb{E}[f(X)|A]], \quad (1)$$

$$\text{EOG}_f(A) = \mathbb{E}[\mathbb{E}[f(X)|Y] - \mathbb{E}[f(X)|Y, A]], \quad (2)$$

$$\text{GSG}_f(A) = \mathbb{E}[\mathbb{E}[Y | f(X)] - \mathbb{E}[Y | f(X), A]]. \quad (3)$$

## 4 Method

The existing fairness notion in CCA [45] ensures that the local models learned from each group maintain a consistent distance from the global model in terms of correlation. However, this does not directly guarantee fairness for subsequent tasks, such as fairness-aware classification using notions such as demographic parity (DP), equalized odds (EO) or group sufficiency (GS) [10, 32, 34]. This is because these fairness notions require that the classification predictions should not be influenced by the sensitive attribute, whereas previous fair CCA is not optimized for that purpose. To satisfy this point, an appealing approach is *fair representation learning* [42]. Let  $\mathbf{x} \in \mathcal{X}$  denote a random vector representing features based on which predictions are made. The idea of fair representation learning is to learn a fair feature representation  $f : \mathcal{X} \rightarrow \mathcal{X}'$  where  $\mathbf{x}$  is mapped to a new feature space  $f(\mathbf{x}) \in \mathcal{X}'$  such that  $f(\mathbf{x})$  is (approximately) independent of the sensitive attribute. Once a fair representation is found, any model trained on this representation will also be fair in terms of fairness notion in classification, such as

DP, EO, or GS. Of course, the representation still needs to contain some information about  $\mathbf{x}$  in order to be useful.

In our proposed fair CCA-based representation learning (FR-CCA), we remove sensitive information when projecting the dataset onto the  $R$ -dimensional linear subspace. We look for a best approximating projection such that the projected data does not contain sensitive information anymore: let  $\mathbf{z} \in \{0, 1\}^N$  denote the vector containing the sensitive attribute of  $N$  data points and let  $z_i \in \{0, 1\}$  denote its  $i$ th component corresponding to the  $i$ th data point, where the binary value encodes membership in one of two demographic groups and let  $\mathbf{X}_i \in \mathbb{R}^{1 \times D_x}$  and  $\mathbf{Y}_i \in \mathbb{R}^{1 \times D_y}$  denote the  $i$ th row of  $\mathbf{X} \in \mathbb{R}^{N \times D_x}$  and  $\mathbf{Y} \in \mathbb{R}^{N \times D_y}$  which represent the  $i$ th data point from two datasets separately.

Ideally, we aim to prevent any classifier from predicting  $z_i$  based solely on the projection of  $\mathbf{X}_i$  or  $\mathbf{Y}_i$  onto the  $R$ -dimensional subspace. Our goal is to solve the following:

$$\begin{aligned} \max_{\mathbf{U}, \mathbf{V}} \quad & \text{trace}(\mathbf{U}^\top \mathbf{X}^\top \mathbf{Y} \mathbf{V}) \quad \text{subject to} \quad \mathbf{U} \in \mathcal{U}, \mathbf{V} \in \mathcal{V}, \\ \text{where } \mathcal{U} := & \left\{ \mathbf{U} \in \mathbb{R}^{D_x \times R} \mid \mathbf{U}^\top \mathbf{X}^\top \mathbf{X} \mathbf{U} = \mathbf{I}_R; \quad \forall f: \mathbb{R}^R \rightarrow \mathbb{R}, \right. \\ & \left. f(\mathbf{U}^\top \mathbf{X}_i^\top) \text{ and } z_i \text{ are statistically independent} \right\}, \quad (4) \\ \mathcal{V} := & \left\{ \mathbf{V} \in \mathbb{R}^{D_y \times R} \mid \mathbf{V}^\top \mathbf{Y}^\top \mathbf{Y} \mathbf{V} = \mathbf{I}_R; \quad \forall g: \mathbb{R}^R \rightarrow \mathbb{R}, \right. \\ & \left. g(\mathbf{V}^\top \mathbf{Y}_i^\top) \text{ and } z_i \text{ are statistically independent} \right\}. \end{aligned}$$

For a given target dimension  $R$ , the set  $\mathcal{U}$  and  $\mathcal{V}$  defined in (4) may be empty, making the constrained CCA problem undefined due to overly stringent restrictions. These restrictions may fail under general functions  $f$  and  $g$ , as counterexamples exist where the transformed  $i$ th observation and  $z_i$  remain statistically linked. To address this, following [22], we relax (4) by expanding the set  $\mathcal{U}$  and  $\mathcal{V}$  in two ways: first, we restrict our goal to linear functions of the form

$$f(\mathbf{a}) = \mathbf{w}_1^\top \mathbf{a} + b_1 \quad \text{and} \quad g(\mathbf{a}) = \mathbf{w}_2^\top \mathbf{a} + b_2 \quad (5)$$

where  $\mathbf{w}_1, \mathbf{w}_2 \in \mathbb{R}^R$  and  $b_1, b_2 \in \mathbb{R}$ ; second, rather than requiring  $f(\mathbf{U}^\top \mathbf{X}_i^\top)$  and  $z_i$  to be independent, we only require the two variables to be uncorrelated, that is their covariance to be zero. The same requirement applies to  $g(\mathbf{V}^\top \mathbf{Y}_i^\top)$  and  $z_i$ . This leaves us with the following problem:

$$\begin{aligned} \max_{\mathbf{U}, \mathbf{V}} \quad & \text{trace}(\mathbf{U}^\top \mathbf{X}^\top \mathbf{Y} \mathbf{V}) \quad \text{subject to} \quad \mathbf{U} \in \mathcal{U}', \mathbf{V} \in \mathcal{V}', \\ \text{where } \mathcal{U}' := & \left\{ \mathbf{U} \in \mathbb{R}^{D_x \times R} \mid \mathbf{U}^\top \mathbf{X}^\top \mathbf{X} \mathbf{U} = \mathbf{I}_R; \right. \\ & \left. \forall \mathbf{w}_1 \in \mathbb{R}^R, b_1 \in \mathbb{R}, \text{Cov}(\mathbf{w}_1^\top \mathbf{U}^\top \mathbf{X}_i^\top + b_1, z_i) = 0 \right\}, \quad (6) \\ \mathcal{V}' := & \left\{ \mathbf{V} \in \mathbb{R}^{D_y \times R} \mid \mathbf{V}^\top \mathbf{Y}^\top \mathbf{Y} \mathbf{V} = \mathbf{I}_R; \right. \\ & \left. \forall \mathbf{w}_2 \in \mathbb{R}^R, b_2 \in \mathbb{R}, \text{Cov}(\mathbf{w}_2^\top \mathbf{V}^\top \mathbf{Y}_i^\top + b_2, z_i) = 0 \right\}. \end{aligned}$$

Here, the “Cov( $\mathbf{x}, \mathbf{y}$ )” refers to the covariance between  $\mathbf{x}$  and  $\mathbf{y}$ .

It can be seen that Problem (6) is well-defined. The optimization can be solved analytically similarly to standard CCA: with  $\bar{\mathbf{z}} =$

---

#### Algorithm 1 FR-CCA and Subsequent Classification

---

**Require:** Modalities  $\mathbf{X} \in \mathbb{R}^{N \times D_x}$ ,  $\mathbf{Y} \in \mathbb{R}^{N \times D_y}$ ; Sensitive attribute  $\mathbf{z} \in \mathbb{R}^N$ ; Label  $\mathbf{y} \in \mathbb{R}^N$

**Ensure:** Projected modalities  $\mathbf{X}_{\text{fair}}, \mathbf{Y}_{\text{fair}}$ ; Classification results

##### Part 1: Learn Fair Representation

- 1: Standardize  $\mathbf{X}$ ,  $\mathbf{Y}$ , and  $\mathbf{z}$
- 2: Perform SVD on  $\mathbf{X}^\top \mathbf{z}$ :  $[\mathbf{U}_x, \Sigma_x, \mathbf{V}_x^\top] = \text{SVD}(\mathbf{X}^\top \mathbf{z})$
- 3: Perform SVD on  $\mathbf{Y}^\top \mathbf{z}$ :  $[\mathbf{U}_y, \Sigma_y, \mathbf{V}_y^\top] = \text{SVD}(\mathbf{Y}^\top \mathbf{z})$
- 4: Set  $\mathbf{R}_x = \mathbf{U}_x^\top[:, 1:]$  and  $\mathbf{R}_y = \mathbf{U}_y^\top[:, 1:]$
- 5: Project data to null spaces:  $\mathbf{X}_{\text{new}} = \mathbf{X} \mathbf{R}_x$ ,  $\mathbf{Y}_{\text{new}} = \mathbf{Y} \mathbf{R}_y$
- 6: Fit CCA on projected data:  $\Lambda_x, \Lambda_y = \text{CCA}(\mathbf{X}_{\text{new}}, \mathbf{Y}_{\text{new}})$
- 7: Calculate  $\mathbf{U} = \mathbf{R}_x \Lambda_x$ ,  $\mathbf{V} = \mathbf{R}_y \Lambda_y$
- 8: Transform data:  $\mathbf{X}_{\text{fair}} = \mathbf{X} \mathbf{U}$ ,  $\mathbf{Y}_{\text{fair}} = \mathbf{Y} \mathbf{V}$

##### Part 2: Subsequent Classification

- 9: Train a classifier (e.g., SVM) on  $\mathbf{X}_{\text{fair}}$  with labels  $\mathbf{y}$
  - 10: Train a classifier (e.g., SVM) on  $\mathbf{Y}_{\text{fair}}$  with labels  $\mathbf{y}$
  - 11: Compute fairness metrics: EOG, GSG, DPG
- 

$\frac{1}{N} \sum_{i=1}^N z_i$  and  $\hat{\mathbf{z}} = (z_1 - \bar{z}, \dots, z_N - \bar{z})^\top \in \mathbb{R}^N$  such that

$$\begin{aligned} \forall \mathbf{w}_1 \in \mathbb{R}^R, b_1 \in \mathbb{R} : & \mathbf{w}_1^\top \mathbf{U}^\top \mathbf{X}_i^\top + b_1 \text{ and } z_i \text{ are uncorrelated} \\ \Leftrightarrow \forall \mathbf{w}_1 \in \mathbb{R}^R, b_1 \in \mathbb{R} : & \sum_{i=1}^N (z_i - \bar{z}) \cdot (\mathbf{w}_1^\top \mathbf{U}^\top \mathbf{X}_i^\top + b_1) = 0 \\ \Leftrightarrow \forall \mathbf{w}_1 : & \mathbf{w}_1^\top \mathbf{U}^\top \mathbf{X}^\top \hat{\mathbf{z}} = 0 \Leftrightarrow \mathbf{U}^\top \mathbf{X}^\top \hat{\mathbf{z}} = \mathbf{0}, \end{aligned}$$

where we ignore  $b_1$  since it is arbitrary and independent of  $\hat{\mathbf{z}}$ . Similarly we have  $\mathbf{V}^\top \mathbf{Y}^\top \hat{\mathbf{z}} = \mathbf{0}$ . We assume that  $\mathbf{X}^\top \hat{\mathbf{z}} \neq \mathbf{0}$  and  $\mathbf{Y}^\top \hat{\mathbf{z}} \neq \mathbf{0}$ . Let  $\mathbf{R}_x \in \mathbb{R}^{D_x \times (D_x - 1)}$  and  $\mathbf{R}_y \in \mathbb{R}^{D_y \times (D_y - 1)}$  comprise as columns an orthonormal basis of the nullspace of  $\mathbf{X}^\top \hat{\mathbf{z}}$  and  $\mathbf{Y}^\top \hat{\mathbf{z}}$ , respectively. Every  $\mathbf{U} \in \mathcal{U}'$  and  $\mathbf{V} \in \mathcal{V}'$  can then be written as

$$\mathbf{U} = \mathbf{R}_x \Lambda_x \text{ and } \mathbf{V} = \mathbf{R}_y \Lambda_y \quad (7)$$

where  $\Lambda_x \in \mathbb{R}^{(D_x - 1) \times R}$  with  $\Lambda_x^\top \Lambda_x = \mathbf{I}_R$  and  $\Lambda_y \in \mathbb{R}^{(D_y - 1) \times R}$  with  $\Lambda_y^\top \Lambda_y = \mathbf{I}_R$ . Then the objective in (6) becomes

$$\text{trace}(\Lambda_x^\top \mathbf{R}_x^\top \mathbf{X}^\top \mathbf{Y} \mathbf{R}_y \Lambda_y), \quad (8)$$

where we now maximize w.r.t.  $\Lambda_x$  and  $\Lambda_y$ . The latter problem has exactly the form of CCA with  $\mathbf{X}$  replaced by  $\mathbf{X} \mathbf{R}_x$  and  $\mathbf{Y}$  replaced by  $\mathbf{Y} \mathbf{R}_y$ . Once we have  $\Lambda_x$  and  $\Lambda_y$ , we obtain a solution  $\mathbf{U}$  and  $\mathbf{V}$  of (6) by computing  $\mathbf{U} = \mathbf{R}_x \Lambda_x$  and  $\mathbf{V} = \mathbf{R}_y \Lambda_y$ . The final optimization problem of FR-CCA is to find  $\mathbf{U} \in \mathbb{R}^{D_x \times R}$  and  $\mathbf{V} \in \mathbb{R}^{D_y \times R}$  such that

$$\begin{aligned} \max \quad & \text{trace}(\mathbf{U}^\top \mathbf{X}^\top \mathbf{Y} \mathbf{V}) \\ \text{subject to} \quad & \mathbf{U}^\top \mathbf{X}^\top \mathbf{X} \mathbf{U} = \mathbf{V}^\top \mathbf{Y}^\top \mathbf{Y} \mathbf{V} = \mathbf{I}_R, \quad (\text{FR-CCA}) \\ & \mathbf{U}^\top \mathbf{X}^\top \hat{\mathbf{z}} = \mathbf{V}^\top \mathbf{Y}^\top \hat{\mathbf{z}} = \mathbf{0}. \end{aligned}$$

After we have the new fair representations for the two modalities, i.e.  $\mathbf{X}_{\text{fair}} = \mathbf{X} \mathbf{U}$  and  $\mathbf{Y}_{\text{fair}} = \mathbf{Y} \mathbf{V}$ , we can easily train classifiers on both representations with the same label  $\mathbf{y}$ . The detailed procedure is summarized in Algorithm 1.

## 5 Time Complexity Analysis

The analysis of the time complexity of the FR-CCA algorithm, which primarily involves Singular Value Decomposition (SVD), matrix multiplication, and classical CCA, yields the following observations:

- (1) **Time Complexity of SVD:** The time complexity of SVD is determined by the size of the data matrix's variables, with a complexity of  $O(D_x + D_y)$ .
- (2) **Time Complexity of Projecting Data Matrix to Null Spaces:** Projecting the data matrix to the null spaces has a time complexity of  $O(N \cdot D_x \cdot (D_x - 1) + N \cdot D_y \cdot (D_y - 1))$ .
- (3) **Time Complexity of Classical CCA:** The time complexity of classical Canonical Correlation Analysis (CCA) can be divided into two main components: (a) *Covariance Matrix Calculation:* The complexity of computing the covariance matrix is  $O(N \cdot D_x^2 + N \cdot D_y^2 + N \cdot D_x \cdot D_y)$ . (b) *Eigenvalue Decomposition:* The complexity of the eigenvalue decomposition is  $O((D_x + D_y)^3)$ . Combining these two components, the overall time complexity for classical CCA is  $O((D_x + D_y)^3 + N \cdot D_x^2 + N \cdot D_y^2 + N \cdot D_x \cdot D_y)$ .

In summary, the time complexity of the classical CCA algorithm, as described in Item (3) mentioned above, dominates the overall complexity of the algorithm. Therefore, the FR-CCA algorithm shares the same time complexity as classical CCA, which is  $O((D_x + D_y)^3 + N \cdot D_x^2 + N \cdot D_y^2 + N \cdot D_x \cdot D_y)$ .

## 6 Experiments

### 6.1 Datasets

**6.1.1 Synthetic Data.** Following [4, 28], we employ multivariate Gaussian distribution to generate the data matrices  $\mathbf{X} \in \mathbb{R}^{N \times D_x}$  and  $\mathbf{Y} \in \mathbb{R}^{N \times D_y}$ , integrating strong relationships with the sensitive attribute  $\mathbf{z} \in \mathbb{R}^N$ . To achieve this, we take the exponential of a linear combination of odd-indexed and even-indexed features from  $\mathbf{X}$  and  $\mathbf{Y}$ , subsequently blending these exponentiated components to form  $\mathbf{z}$ . Then, the mean of  $\mathbf{z}$  across all samples is considered as the threshold to distinguish the sensitive subgroups. This process enhances the correlation between  $\mathbf{z}$  and the data features. For label generation, we combine the first half of the features from  $\mathbf{X}$ , the latter half from  $\mathbf{Y}$ , and the exponential of  $\mathbf{z}$ . The mean of the aggregate serves as the binarization threshold, creating binary labels that simulate a potential sensitive bias within the dataset. The design mimics real-world scenarios where sensitive attributes may unfairly influence predictions, such as sex bias in Alzheimer's diagnosis. This synthetic data allows us to highlight the efficiency of FR-CCA in mitigating unfairness in classification tasks.

The synthetic data are generated by employing a multivariate Gaussian distribution. This formulation is given as follows:

$$\begin{pmatrix} \mathbf{X} \\ \mathbf{Y} \end{pmatrix} \sim \mathcal{N} \left( \begin{bmatrix} \mu_x \\ \mu_y \end{bmatrix}, \begin{bmatrix} \Sigma_x & \Sigma_{xy} \\ \Sigma_{yx} & \Sigma_y \end{bmatrix} \right), \quad (9)$$

where  $\mu_x \in \mathbb{R}^{D_x}$  and  $\mu_y \in \mathbb{R}^{D_y}$  denote the mean vectors for the data matrices  $\mathbf{X}$  and  $\mathbf{Y}$ , correspondingly; covariance matrices  $\Sigma_x$ ,  $\Sigma_y$  and the cross-covariance matrix  $\Sigma_{xy}$  are constructed as follows. Given orthogonal projection matrices  $\mathbf{U} \in \mathbb{R}^{D_x \times R}$ ,  $\mathbf{V} \in \mathbb{R}^{D_y \times R}$ , from the Haar distribution, and canonical correlations  $\boldsymbol{\rho} = (\rho_1, \rho_2, \dots, \rho_R)$  defined as  $\boldsymbol{\rho} = \text{diag}(\mathbf{U}^\top \mathbf{X}^\top \mathbf{Y} \mathbf{V})$ . Let  $\mathbf{U} = \mathbf{Q}_x \mathbf{R}_x$  and  $\mathbf{V} = \mathbf{Q}_y \mathbf{R}_y$  be the QR decomposition of  $\mathbf{U}$  and  $\mathbf{V}$ , then we have

$$\begin{aligned} \Sigma_{xy} &= \Sigma_x \mathbf{U} \text{diag}(\boldsymbol{\rho}) \mathbf{V}^\top \Sigma_y \\ \Sigma_x &= \mathbf{Q}_x (\mathbf{R}_x^\top)^+ \mathbf{R}_x^+ + \epsilon_x (\mathbf{I}_{D_x} - \mathbf{Q}_x \mathbf{Q}_x^\top) \\ \Sigma_y &= \mathbf{Q}_y (\mathbf{R}_y^\top)^+ \mathbf{R}_y^+ + \epsilon_y (\mathbf{I}_{D_y} - \mathbf{Q}_y \mathbf{Q}_y^\top) \end{aligned}$$

Here,  $\epsilon_x$  and  $\epsilon_y$  denote the Gaussian noise levels;  $\mathbf{A}^+$  represents the Moore-Penrose inverse of matrix  $\mathbf{A}$ .

To simulate the sex subgroups within the synthetic dataset, the sensitive attribute  $\mathbf{z}$  is constructed as follows: Let  $\mathbf{X}_{\text{odd}}$  and  $\mathbf{Y}_{\text{even}}$  represent the matrices containing the odd-indexed features of  $\mathbf{X}$  and the even-indexed features of  $\mathbf{Y}$  respectively. We define the sensitive attribute value of sample  $i$  by:

$$z_i = \alpha \exp \left( \sum_j a_j \mathbf{X}_{\text{odd},ij} \right) + \beta \exp \left( \sum_k b_k \mathbf{Y}_{\text{even},ik} \right), \quad (10)$$

where  $\alpha$  and  $\beta$  are weights determining the contribution of each modality to the sensitive attribute, and  $a_j, b_k$  are the coefficients of the linear combinations. The attribute  $\mathbf{z}$  is then binarized based on:

$$z_i = \begin{cases} 1 & \text{if } z_i \leq \tau \\ 2 & \text{if } z_i > \tau \end{cases}, \text{ where } \tau = \frac{1}{N} \sum_{i=1}^N z_i. \quad (11)$$

This binarization splits the dataset into two subgroups, intended to simulate sex divisions, and is utilized to assess the model's fairness in handling sex-related biases.

To generate the labels  $\mathbf{y} \in \mathbb{R}^N$ , we first define the combined feature vector  $\mathbf{c} \in \mathbb{R}^N$  as:

$$\mathbf{c} = \sum_{i=1}^{\lfloor \frac{D_x}{2} \rfloor} \mathbf{X}_{:,i} + \sum_{j=\lfloor \frac{D_y}{2} \rfloor}^{D_y} \mathbf{Y}_{:,j} + \exp(\mathbf{z}) \quad (12)$$

where  $\mathbf{X}_{:,i}, \mathbf{Y}_{:,i}$  represents the  $i$ th column of  $\mathbf{X}, \mathbf{Y}$  respectively and  $\lfloor \cdot \rfloor$  denotes the floor function which returns the greatest integer less than or equal to its argument. The binary label for each instance is then given by:

$$y_i = \begin{cases} 1 & \text{if } c_i \leq t \\ 2 & \text{if } c_i > t \end{cases}, \text{ where } t = \frac{1}{N} \sum_{i=1}^N c_i. \quad (13)$$

As shown in Table 2, our synthetic datasets refer to two modalities  $\mathbf{X}$  and  $\mathbf{Y}$ , where  $\mathbf{X}$  contains 55 features and  $\mathbf{Y}$  comprises 60 features. These datasets include 500 samples divided into 304 positive and 196 negative cases. The distribution of participants into two sensitive groups, with 398 in Group 1 and 102 in Group 2, allows for comprehensive modeling and validation of diagnostic algorithms. The synthetic datasets provide a controlled environment to evaluate the robustness and generalizability of predictive models developed using the ADNI datasets.

**6.1.2 Real Data.** Our experiment incorporates two medical imaging modalities: (1) Magnetic Resonance Imaging (MRI) scans and (2) Tau (AV1451) positron emission tomography (PET) scans from the Alzheimer's Disease Neuroimaging Initiative (ADNI) database [35, 36]. The ADNI was launched in 2003 as a public-private partnership led by Principal Investigator Michael W. Weiner, MD. ADNI aims to determine if serial magnetic resonance imaging (MRI), positron emission tomography (PET), other biological markers, and clinical and neuropsychological assessments can be integrated to track the progression of MCI and early AD. (<http://adni.loni.usc.edu>)

Table 2 shows that the dataset comprises 375 subjects (182 males, 193 females), with 66 cortical thickness features from MRI and 68 cortical standardized uptake value ratio (SUVR) features measuring

Table 1: Numerical results (mean $\pm$ std) in terms of three fairness metrics of SVM, CCA, SF-CCA, MF-CCA and our FR-CCA (the smaller the better). The best one for each modality in each line among the five methods is in bold.

Modality	Metric	SVM	CCA	SF-CCA	MF-CCA	FR-CCA
Synthetic X	GSG	0.303 $\pm$ 0.009	0.278 $\pm$ 0.023	0.301 $\pm$ 0.015	0.307 $\pm$ 0.026	<b>0.242 <math>\pm</math> 0.046</b>
	DPG	0.102 $\pm$ 0.047	0.077 $\pm$ 0.056	0.089 $\pm$ 0.022	0.099 $\pm$ 0.050	<b>0.026 <math>\pm</math> 0.031</b>
	EOG	0.103 $\pm$ 0.127	0.064 $\pm$ 0.049	0.077 $\pm$ 0.070	0.114 $\pm$ 0.140	<b>0.012 <math>\pm</math> 0.014</b>
	Precision	0.600 $\pm$ 0.016	0.591 $\pm$ 0.019	0.606 $\pm$ 0.045	0.612 $\pm$ 0.028	<b>0.635 <math>\pm</math> 0.022</b>
	Recall	0.495 $\pm$ 0.020	0.457 $\pm$ 0.083	0.508 $\pm$ 0.084	0.534 $\pm$ 0.083	<b>0.599 <math>\pm</math> 0.029</b>
	ROC-AUC Score	0.493 $\pm$ 0.017	0.486 $\pm$ 0.017	0.479 $\pm$ 0.048	<b>0.536 <math>\pm</math> 0.049</b>	0.532 $\pm$ 0.032
Synthetic Y	GSG	0.274 $\pm$ 0.038	0.329 $\pm$ 0.042	0.286 $\pm$ 0.009	0.296 $\pm$ 0.004	<b>0.216 <math>\pm</math> 0.084</b>
	DPG	0.075 $\pm$ 0.069	0.081 $\pm$ 0.040	0.100 $\pm$ 0.069	0.104 $\pm$ 0.057	<b>0.037 <math>\pm</math> 0.035</b>
	EOG	0.107 $\pm$ 0.131	0.084 $\pm$ 0.037	0.077 $\pm$ 0.076	0.095 $\pm$ 0.117	<b>0.022 <math>\pm</math> 0.010</b>
	Precision	0.624 $\pm$ 0.026	0.612 $\pm$ 0.033	0.632 $\pm$ 0.038	<b>0.645 <math>\pm</math> 0.029</b>	0.596 $\pm$ 0.054
	Recall	0.523 $\pm$ 0.069	<b>0.612 <math>\pm</math> 0.033</b>	0.477 $\pm$ 0.073	0.512 $\pm$ 0.053	0.569 $\pm$ 0.017
	ROC-AUC Score	0.519 $\pm$ 0.030	<b>0.811 <math>\pm</math> 0.016</b>	0.508 $\pm$ 0.084	0.537 $\pm$ 0.030	0.525 $\pm$ 0.037
ADNI MRI	GSG	0.329 $\pm$ 0.042	0.302 $\pm$ 0.230	0.286 $\pm$ 0.033	0.296 $\pm$ 0.004	<b>0.258 <math>\pm</math> 0.038</b>
	DPG	0.081 $\pm$ 0.040	0.026 $\pm$ 0.032	0.036 $\pm$ 0.024	0.104 $\pm$ 0.057	<b>0.010 <math>\pm</math> 0.011</b>
	EOG	0.084 $\pm$ 0.037	0.020 $\pm$ 0.018	0.033 $\pm$ 0.031	0.095 $\pm$ 0.117	<b>0.014 <math>\pm</math> 0.011</b>
	Precision	0.612 $\pm$ 0.033	0.552 $\pm$ 0.627	0.619 $\pm$ 0.026	<b>0.645 <math>\pm</math> 0.029</b>	0.611 $\pm$ 0.014
	Recall	0.612 $\pm$ 0.033	0.552 $\pm$ 0.063	<b>0.619 <math>\pm</math> 0.026</b>	0.512 $\pm$ 0.053	0.611 $\pm$ 0.014
	ROC-AUC Score	<b>0.811 <math>\pm</math> 0.016</b>	0.782 $\pm$ 0.017	0.800 $\pm$ 0.020	0.537 $\pm$ 0.030	0.773 $\pm$ 0.027
ADNI AV1451	GSG	0.329 $\pm$ 0.042	0.239 $\pm$ 0.208	0.286 $\pm$ 0.033	0.242 $\pm$ 0.042	<b>0.215 <math>\pm</math> 0.041</b>
	DPG	0.081 $\pm$ 0.040	0.028 $\pm$ 0.024	0.036 $\pm$ 0.024	0.015 $\pm$ 0.013	<b>0.008 <math>\pm</math> 0.006</b>
	EOG	0.084 $\pm$ 0.037	0.015 $\pm$ 0.017	0.033 $\pm$ 0.031	0.026 $\pm$ 0.022	<b>0.010 <math>\pm</math> 0.005</b>
	Precision	0.612 $\pm$ 0.033	<b>0.635 <math>\pm</math> 0.026</b>	0.619 $\pm$ 0.026	0.621 $\pm$ 0.015	0.612 $\pm$ 0.009
	Recall	0.612 $\pm$ 0.033	<b>0.635 <math>\pm</math> 0.026</b>	0.619 $\pm$ 0.026	0.621 $\pm$ 0.015	0.612 $\pm$ 0.009
	ROC-AUC Score	<b>0.811 <math>\pm</math> 0.016</b>	0.791 $\pm$ 0.020	0.800 $\pm$ 0.020	0.769 $\pm$ 0.024	0.798 $\pm$ 0.020
Summary	Win Times	2	4	1	3	14

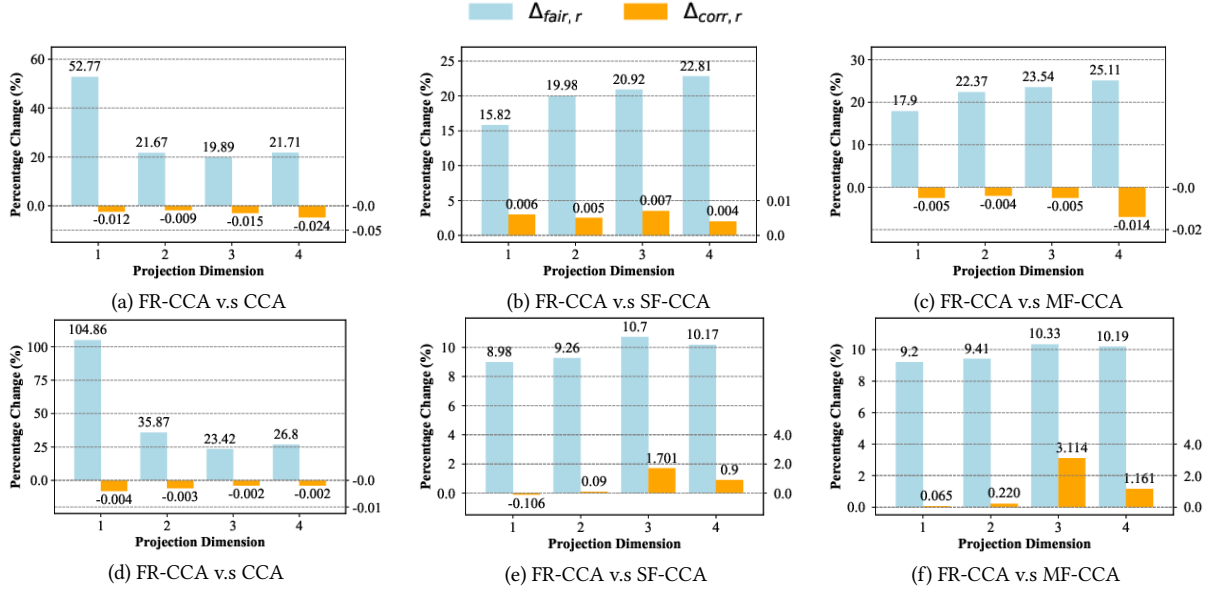


Figure 2: Percentage change of correlation and fairness from baseline CCA methods to FR-CCA on synthetic data (top line) and ADNI data (bottom line) in unsupervised learning. Our FR-CCA achieves a significant improvement in fairness ( $\gamma_r$ ) while experiencing minor or even no loss in correlation ( $\rho_r$ ).

tau accumulation level from AV1451 scans. Label distribution is categorized into cognitive normal (CN, N=224), mild cognitive impairment (MCI, N=121), and Alzheimer’s Disease subjects (AD, N=30).

ADNI data are analyzed to explore fair representation through FR-CCA and its impact on subsequent medical imaging classification tasks, with a focus on sex-based subgroup fairness.

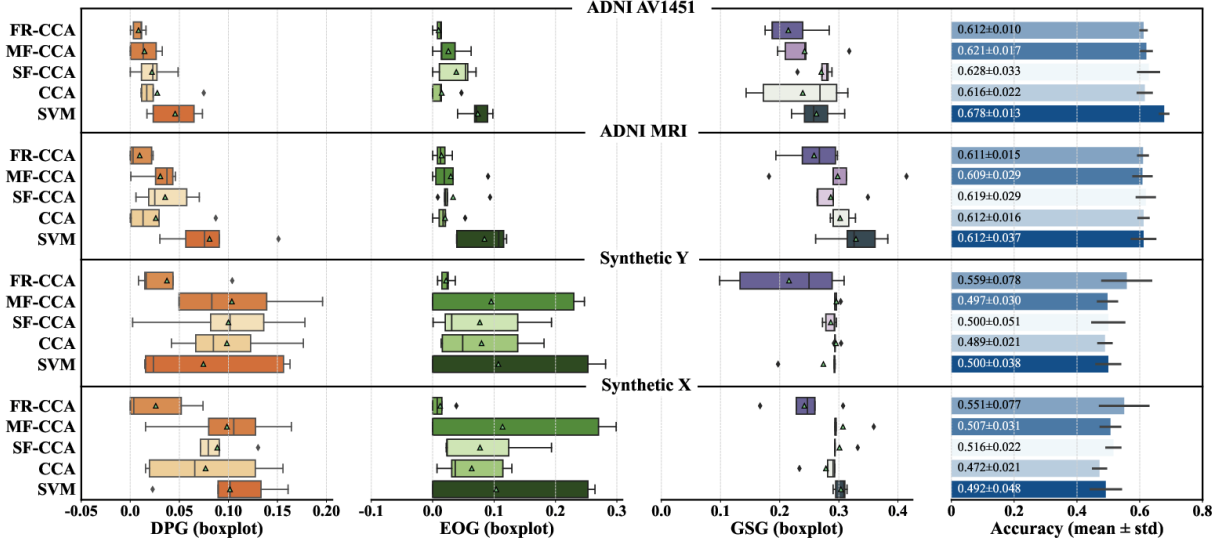


Figure 3: Comparison plot for fairness metrics (DPG, EOG, GSG) and Accuracy on four modalities (X and Y for synthetic data, MRI and AV1451 for ADNI data). We use boxplots to illustrate the results for three fairness metrics as they exhibit significant variation across different methods. We use boxplots to display the accuracy, as there is minimal variation across different methods. The green triangle represents the mean value over five runs in the boxplots, and the dark diamonds refer to outliers. Our FR-CCA outperforms all the baseline models regarding three fairness metrics (the smaller, the better) while also achieving competitive accuracy results (the larger, the better).

Table 2: Demographic and diagnostic breakdown of the ADNI (MRI and AV1451) and synthetic datasets (X and Y).

Dataset	ADNI: MRI vs. AV1451				Synthetic: X vs. Y		
Diagnosis/ Label	CN	MCI	AD	Total	Positive	Negative	Total
	224	121	30	375	304	196	500
Sensitive Attribute	Male		Female		Group 1		Group 2
	193		182		398		102

where “(p)” refers to the proposed method and “(b)” refers to a baseline method. In this unsupervised scenario, we define

$$\gamma_x = U^T X^T \hat{z}, \quad \gamma_y = V^T Y^T \hat{z} \quad (16)$$

in X, Y respectively (refer to (FR-CCA)), and then the fairness metric for  $r$ th dimension in CCA task (unsupervised learning phase) is defined by

$$\gamma_r = \frac{[\gamma_x]_r + [\gamma_y]_r}{2}. \quad (17)$$

Then, the percentage change of fairness is given by:

$$\Delta_{\text{fair},r} = -\frac{\gamma_r^{(p)} - \gamma_r^{(b)}}{\gamma_r^{(b)}} \times 100\%. \quad (18)$$

## 6.2 Setting

Our experimental framework involves two stages: an unsupervised learning phase focused on discovering a meaningful representation, followed by a subsequent classification task. In the unsupervised learning stage, FR-CCA’s performance is evaluated on the percentage change of correlation and fairness compared to CCA, SF-CCA, and MF-CCA for  $r$ th dimension of representation spaces, where  $r = 1, \dots, R$ . Let  $U = [u_1, \dots, u_R] \in \mathbb{R}^{D_x \times R}$  and  $V = [v_1, \dots, v_R] \in \mathbb{R}^{D_y \times R}$ , and then the  $r$ th canonical correlation, is formulated as:

$$\rho_r = \frac{u_r^T X^T Y v_r}{\sqrt{u_r^T X^T X u_r v_r^T Y^T Y v_r}}. \quad (14)$$

Then, the percentage change of correlation is given by:

$$\Delta_{\text{corr},r} = \frac{\rho_r^{(p)} - \rho_r^{(b)}}{\rho_r^{(b)}} \times 100\%, \quad (15)$$

In the subsequent classification task, we employ support vector machine (SVM) [33] for classification, which is robust and effective in handling datasets with complicated structures. We also train logistic regression (LR) and multiple-layer perceptron (MLP) models on these fair representations and put their results in Appendix A.1. To assess the performance of the classifier, we focus on four metrics (refer to Section 3): Demographic Parity Gap (DPG), Equalized Odds Gap (EOG), Group Sufficiency Gap (GSG), and Accuracy. A discussion on why we choose these fairness metrics can be found in Appendix B.1.

For hyperparameter tuning, a specific random seed is allocated for optimal parameter selection. The dataset is divided into a training set (70%) and a testing set (30%). Stratified 5-fold cross-validation is applied to the training dataset. Subsequently, a random search is conducted using three distinct scorers-DPG, EOG, and GSG-each is



designed to measure the model’s performance against fairness metrics. We utilize kernels such as Sigmoid and Radial Basis Function (RBF) due to the non-linear separability of the dataset and uniform distribution to search for the optimal parameters: the penalty parameter  $C \in [0.1, 200]$ , the kernel coefficient  $\gamma \in [0.1, 200]$  along with “scale” and “auto” options, and the kernel coefficient  $\text{coef0} \in [0, 50]$  (“Sigmoid” only). In the actual training phase, we use five additional seeds to split the data into training (70%) and testing (30%) sets with the optimally tuned hyperparameters from the previous step to train the model. The final evaluation criteria are based on the mean and standard deviation of outcomes across these seeds, offering a comprehensive assessment of the model’s fairness, accuracy, performance, and robustness. This methodology ensures a balanced evaluation that reflects the model’s ability to generalize across different datasets while retaining fair and accurate predictions.

### 6.3 Baselines

To evaluate the effectiveness and fairness of our proposed FR-CCA, we compare its performance against two fairness-enhanced CCA methods and two foundational baselines. SF-CCA and MF-CCA [45] are included to benchmark fairness metrics. Foundational CCA [15] serves as a baseline to demonstrate the contrast in maximizing correlation without the fairness enhancement. Additionally, an SVM classifier trained on the original data acts as a performance benchmark, highlighting the effects of preprocessing steps on raw prediction. This diverse set of baselines allows us to highlight FR-CCA’s ability to improve fairness without sacrificing the correlation and predicting accuracy. We also compare our method with methods that focus solely on fair classification and the results can be found in Appendix A.2. The discussion on the key difference between our FR-CCA and F-CCA can be found in Appendix B.3.

### 6.4 Results

**6.4.1 Results on synthetic data.** In the simulation experiment, we follow the methodology demonstrated in Section 4.1 to generate two synthetic datasets  $\mathbf{X} \in \mathbb{R}^{N \times D_x}$ ,  $\mathbf{Y} \in \mathbb{R}^{N \times D_y}$  with  $N = 500$ ,  $D_x = 55$ ,  $D_y = 60$ , along with sensitive attributes  $\mathbf{z}$  and labels by the given ground truth projection matrices  $\mathbf{U} \in \mathbb{R}^{D_x \times R}$ ,  $\mathbf{V} \in \mathbb{R}^{D_y \times R}$ , and canonical correlation  $\rho = [0.8, 0.6, 0.3, 0.5]$ .

The unsupervised learning stage compares FR-CCA with three baselines: CCA, SF-CCA, and MF-CCA. Figure 2(a,b,c) shows the percentage change in fairness and correlation when using FR-CCA compared to the baselines across various dimensions. FR-CCA demonstrates significant improvements in fairness, with slight decreases or even no loss compared to all three baselines.

We run the experiment on  $R = 2$  dimension in the subsequent classification task. As shown in Figure 3 (bottom two lines), FR-CCA significantly outperforms other algorithms in reducing DPG, EOG, and GSG, suggesting an obvious mitigation of bias across distinct sensitive subgroups while keeping competitive accuracy, illustrating a balanced trade-off between fairness and accuracy in the prediction task. FR-CCA performs well on both Synthetic X and Synthetic Y modalities by achieving high precision, recall, and ROC-AUC scores, demonstrating its capability to match other methods in traditional performance metrics while significantly enhancing fairness. This balance of performance and fairness makes FR-CCA a

superior choice for equitable and accurate prediction. The numerical values (mean $\pm$ std) of the three fairness metrics and accuracy are presented in Table 1 (first two rows) and Figure 3 (first two rows, last column), respectively. The discussion on the choice of  $R$  can be found in Appendix B.4.

**6.4.2 Results on real data.** The analysis of ADNI data strictly follows the steps in synthetic data. As depicted in Figure 2(d,e,f), FR-CCA remains a significant improvement of fairness with almost no loss of correlation compared to other baselines across various dimensions in the unsupervised learning phase.

We apply the subsequent classification tasks on MRI and AV1451 modalities separately. As illustrated in Figure 3 (top two rows), our approach not only preserves the predicting accuracy but also significantly reduces the sex-biased prediction. Low GSG, DPG, and EOG values are crucial in Alzheimer’s disease diagnosis as they indicate minimal bias and high fairness across different demographic groups. This ensures that the diagnostic tool provides equitable and accurate patient assessments, leading to more consistent and reliable diagnoses. Reducing these gaps helps prevent misdiagnosis and underdiagnosis in historically disadvantaged populations, ultimately supporting better, more inclusive healthcare outcomes. Additionally, the standard deviation of results by FR-CCA across distinct random seeds is notably small, indicating FR-CCA’s superior robustness in classification tasks.

The overall performance of FR-CCA on both the ADNI MRI and ADNI AV1451 datasets suggests that it is a highly effective method for diagnosing Alzheimer’s disease. Its strength lies in its ability to maintain a balanced and high performance across precision and recall, which is essential for clinical applicability. By effectively minimizing both false positives and false negatives, FR-CCA ensures that patients receive accurate diagnoses, which is critical for timely and appropriate treatment interventions.

The consistently high ROC-AUC scores across different modalities indicate that FR-CCA is reliable and capable of generalizing well, making it a valuable tool in the clinical setting. This method’s ability to provide robust performance metrics highlights its potential for integration into diagnostic workflows, ultimately contributing to improved patient outcomes in Alzheimer’s disease management.

Briefly, the balanced performance of FR-CCA across traditional metrics and fairness metrics suggests it is well-suited for integration into clinical workflows. The numerical values (mean $\pm$ std) of the three fairness metrics and accuracy are presented in Table 1 (last two rows) and Figure 3 (last two rows, last column), respectively. A trade-off discussion between accuracy and fairness can be found in Appendix B.2.

**6.4.3 Hypothesis Testing.** To validate the FR-CCA’s fairness performance against the traditional CCA, we conduct hypothesis tests on the same samples by performing 50 seeds across four modalities for both methods. Our goal is to determine if the FR-CCA significantly improves fairness by reducing GSG, DPG, and EOG compared to CCA. As depicted in Table 4, we also apply Shapiro-Wilk test to check the normality of the distributions before selecting appropriate statistical tests. The detailed procedure for conducting rigorous hypothesis testing is included in the Appendix A.3. For each fairness metric, we set the following hypotheses: (a) **Null Hypothesis  $H_0$ :** The distribution of the fairness metric for the FR-CCA model



**Table 3: Results of hypothesis testing for three fairness metrics—Group Sufficiency (GSG), Demographic Parity (DPG), and Equalized Odds (EOG)—across different modalities: Synthetic X, Synthetic Y, ADNI MRI, and ADNI AV1451. The table includes the test statistics (W for Wilcoxon, T for paired t-test), p-values, and results of the hypothesis tests (Reject  $H_0$  or Not reject  $H_0$ ). A p-value less than 0.05 indicates a statistically significant improvement, leading to the rejection of the null hypothesis  $H_0$ .**

Metric	Synthetic X	Synthetic Y	ADNI MRI	ADNI AV1451
Stats	GSG 131.1 (W)	−2.866 (T)	479.0 (W)	−4.044 (T)
	DPG 325.0 (W)	272.0 (W)	594.0 (W)	105.0 (W)
	EOG 397.0 (W)	−3.128 (T)	−1.108 (T)	56.0 (W)
p-value	GSG $5.245e-08$	$3.058e-03$	$4.998e-02$	$9.291e-05$
	DPG $1.061e-03$	$1.369e-04$	$3.403e-01$	$6.852e-09$
	EOG $9.794e-03$	$1.482e-04$	$3.207e-02$	$1.552e-08$
Result	GSG Reject $H_0$	Reject $H_0$	Reject $H_0$	Reject $H_0$
	DPG Reject $H_0$	Reject $H_0$	Not reject $H_0$	Reject $H_0$
	EOG Reject $H_0$	Reject $H_0$	Reject $H_0$	Reject $H_0$

is not less than that of the baseline CCA model. (b) **Alternative Hypothesis  $H_1$** : The distribution of the fairness metric for the FR-CCA is significantly less than the baseline CCA model. As shown in Table 3 and Supplemental Figure 1, the hypothesis testing results for the GSG, DPG, and EOG across various modalities demonstrate that the FR-CCA generally shows significant improvements, as indicated by the rejection of the null hypothesis in these cases.

**6.4.4 Interpretability Study.** The subsequent prediction task for our FR-CCA model is based on an SVM with an RBF kernel. Unlike a linear SVM, we cannot directly extract the parameter coefficients from the classifier. Therefore, we employ SHAP (SHapley Additive exPlanations) values [25] to calculate the feature importance, which provides a unified measure of feature importance by interpreting the prediction of machine learning models in the low dimensional representation space. We then utilize the projection matrices  $U \in \mathbb{R}^{68 \times 2}$  and  $V \in \mathbb{R}^{66 \times 2}$  learned by FR-CCA to map the feature importance for the first two canonical components back to the original feature spaces, where 68 brain regions for MRI and 66 brain regions for AV1451. Figure 4 shows the important brain regions that our model focuses on in the diagnosis for Alzheimer’s disease. As can be seen, the first row shows the importance of AD risk in all the regions. The second row highlights the top ten important regions for each modality.

For the MRI modality, focusing on neurodegeneration, the most critical regions include those involved in memory, language comprehension, and high-level visual processing. The entorhinal cortex is notably one of the earliest affected areas in AD [18], correlating with significant memory impairment due to its role in memory and navigation. Temporal regions, including the middle and inferior temporal gyri, are vital for semantic memory and language comprehension, and their degeneration leads to comprehension difficulties and memory issues [12]. The degeneration of superior

**Table 4: Time (seconds, mean  $\pm$  std) comparison over 10 experiments across different methods ( $R = 5$  on the ADNI dataset and  $R = 7$  on the synthetic dataset).**

Dataset	CCA	SF-CCA	MF-CCA	FR-CCA
Synthetic	$0.256 \pm 0.008$	$7.322 \pm 1.202$	$31.112 \pm 1.890$	$0.346 \pm 0.011$
ADNI	$0.305 \pm 0.013$	$8.694 \pm 1.574$	$29.382 \pm 2.108$	$0.504 \pm 0.016$

temporal gyrus contributes to language and auditory comprehension deficits [6]. The temporal pole, associated with high-order cognitive functions and relaying information, also shows degeneration, leading to deficits in decision-making and working memory [7]. The fusiform gyrus, essential for high-level visual processing, exacerbates visual recognition deficits upon degeneration [26]. Additionally, the precentral and postcentral gyri show progressive degeneration as AD advances, impacting motor functions and sensory integration [40].

For the AV1451 modality, which assesses tau pathology, the top regions of interest include areas critical for sensory processing, emotional regulation, decision-making, and visual processing. The postcentral gyrus is involved in processing sensory information, and tau accumulation here disrupts sensory perception and processing [1]. The temporal pole is associated with emotional regulation and social cognition with tau accumulation. The rostral anterior cingulate is crucial for emotion regulation and decision-making, and tau pathology here leads to increased apathy and impaired decision-making [17]. The lingual gyrus, important for visual processing, contributes to visual processing deficits when affected by tau. The precentral gyrus, part of the primary motor cortex, leads to a motor dysfunction with tau pathology. The middle and inferior temporal gyri are vital for language and visual object recognition, and tau accumulation exacerbates language comprehension and visual recognition issues [12]. The supramarginal gyrus contributes to language processing deficits with tau accumulation. The heat map visually represents these critical regions, providing a comprehensive understanding of their contributions to AD progression and aiding in accurate disease diagnosis.

**6.4.5 Time Comparison.** Furthermore, we compare the timing performance across CCA, SF-CCA, MF-CCA, and FR-CCA in the unsupervised learning phase shown in Table 4. Note that the experiments are run on 12th Gen Intel(R) Core(TM) i9-12900K 3.19GHz. FR-CCA achieves competitive timing performance compared to CCA, which is consistent with the time analysis in Paragraph 5 and significantly outperforms SF-CCA and MF-CCA, which demonstrates the efficiency and applicability of the proposed method.

## 7 Conclusion

This paper presents a novel fair CCA method that addresses the previous limitations by focusing on fair representation learning. By ensuring the independence of projected features from sensitive attributes, our method achieves improved fairness performance, such as Group Sufficiency Gap (GSG), Demographic Parity Gap (DPG), and Equalized Odds Gap (EOG), without sacrificing accuracy in subsequent classification tasks. The empirical studies conducted on

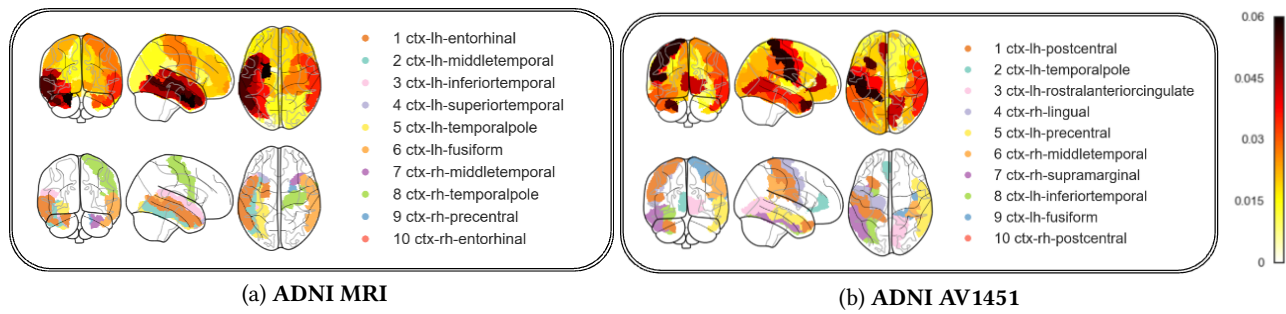


**Figure 4: Brain heat map of feature importance for ADNI MRI and ADNI AV1451 using the coefficient of our FR-CCA model. Each modality includes three slices to display the brain region extensively. The heat maps in the first row showcase all the brain regions of interest (ROI), where darker colors represent greater importance for risk prediction. The second row highlights the top ten significant brain regions in each modality, which are annotated in the legends in the right column.**

both synthetic data and ADNI data demonstrate the effectiveness of the proposed fair CCA method in maintaining high correlation analysis performance while simultaneously enhancing fairness. This novel method excels in traditional performance metrics such as precision, recall, and ROC-AUC scores, ensuring accurate and reliable diagnoses crucial for clinical applications. This balance of high performance and enhanced fairness makes FR-CCA a robust and reliable tool for Alzheimer’s disease diagnosis, promoting equitable healthcare outcomes across diverse patient populations.

## 8 Acknowledgments

This work was supported in part by the NIH grants U01 AG066833, RF1 AG063481, U01 AG068057, R01 LM013463, R01 AG071470 and U19 AG074879.

Data collection and sharing for this project was funded by the Alzheimer’s Disease Neuroimaging Initiative (ADNI) (National Institutes of Health Grant U01 AG024904) and DOD ADNI (Department of Defense award number W81XWH-12-2-0012). ADNI is funded by the National Institute on Aging, the National Institute of Biomedical Imaging and Bioengineering, and through generous contributions from the following: AbbVie, Alzheimer’s Association; Alzheimer’s Drug Discovery Foundation; Araclon Biotech; BioClinica, Inc.; Biogen; Bristol-Myers Squibb Company; CereSpir, Inc.; Cogstate; Eisai Inc.; Elan Pharmaceuticals, Inc.; Eli Lilly and Company; EuroImmun; F. Hoffmann-La Roche Ltd and its affiliated company Genentech, Inc.; Fujirebio; GE Healthcare; IXICO Ltd.; Janssen Alzheimer Immunotherapy Research & Development, LLC.; Johnson & Johnson Pharmaceutical Research & Development LLC.; Lumosity; Lundbeck; Merck & Co., Inc.; Meso Scale Diagnostics, LLC.; NeuroRx Research; Neurotrack Technologies; Novartis Pharmaceuticals Corporation; Pfizer Inc.; Piramal Imaging; Servier; Takeda Pharmaceutical Company; and Transition Therapeutics. The Canadian Institutes of Health Research is providing funds to support ADNI clinical sites in Canada. Private sector contributions are facilitated by the Foundation for the National Institutes of Health ([www.fnih.org](http://www.fnih.org)). The grantee organization is the Northern California Institute for Research and Education, and the study is coordinated by the Alzheimer’s Therapeutic Research Institute at the University of Southern California. ADNI data are disseminated

by the Laboratory for Neuro Imaging at the University of Southern California.

## References

- [1] Samrah Ahmed, Clare Loane, Sara Bartels, Giovanna Zamboni, Clare Mackay, Ian Baker, Masud Husain, Sian Thompson, Michael Hornberger, and Christopher Butler. 2018. Lateral parietal contributions to memory impairment in posterior cortical atrophy. *NeuroImage: Clinical* 20 (07 2018). <https://doi.org/10.1016/j.nicl.2018.07.005>
- [2] Fares Al-Shargie, Tong Boon Tang, and Masashi Kiguchi. 2017. Assessment of mental stress effects on prefrontal cortical activities using canonical correlation analysis: an fNIRS-EEG study. *Biomedical optics express* 8, 5 (2017), 2583–2598.
- [3] Galen Andrew, Raman Arora, Jeff Bilmes, and Karen Livescu. 2013. Deep canonical correlation analysis. In *International conference on machine learning*. PMLR, 1247–1255.
- [4] Francis R Bach and Michael I Jordan. 2005. A probabilistic interpretation of canonical correlation analysis. (2005).
- [5] Solon Barocas, Moritz Hardt, and Arvind Narayanan. 2019. Fairness and Machine Learning. [fairmlbook.org](http://fairmlbook.org).
- [6] Erin Bigler, Sherstin Mortensen, E. Neeley, Sally Ozonoff, Lori Krasny, Michael Johnson, Jeffrey Lu, Sherri Provencal, William McMahon, and Janet Lainhart. 2007. Superior Temporal Gyrus, Language Function, and Autism. *Developmental neuropsychology* 31 (02 2007), 217–38. <https://doi.org/10.1080/87565640701190841>
- [7] Ting-Yu Chen, Jun-Ding Zhu, Shih-Jen Tsai, and Albert Yang. 2024. Exploring morphological similarity and randomness in Alzheimer’s disease using adjacent grey matter voxel-based structural analysis. *Alzheimer’s Research & Therapy* 16 (04 2024). <https://doi.org/10.1186/s13195-024-01448-1>
- [8] Zhiwen Chen, Steven X Ding, Tao Peng, Chunhua Yang, and Weihua Gui. 2017. Fault detection for non-Gaussian processes using generalized canonical correlation analysis and randomized algorithms. *IEEE Transactions on Industrial Electronics* 65, 2 (2017), 1559–1567.
- [9] Alexandra Chouldechova. 2017. Fair prediction with disparate impact: A study of bias in recidivism prediction instruments. *Big data* 5, 2 (2017), 153–163.
- [10] Michele Donini, Luca Oneto, Shai Ben-David, John S Shawe-Taylor, and Massimiliano Pontil. 2018. Empirical risk minimization under fairness constraints. *Advances in neural information processing systems* 31 (2018).
- [11] Cynthia Dwork, Moritz Hardt, Toniann Pitassi, Omer Reingold, and Richard Zemel. 2012. Fairness through awareness. In *Proceedings of the 3rd innovations in theoretical computer science conference*, 214–226.
- [12] Giovanni Frisoni, Nick Fox, Clifford Jack, Ph Scheltens, and Paul Thompson. 2010. The clinical use of structural MRI in Alzheimer’s Disease. *Nature reviews. Neurology* 6 (02 2010), 67–77. <https://doi.org/10.1038/nrneuro.2009.215>
- [13] Moritz Hardt, Eric Price, and Nati Srebro. 2016. Equality of opportunity in supervised learning. *Advances in neural information processing systems* 29 (2016).
- [14] HAROLD HOTELLING. 1936. RELATIONS BETWEEN TWO SETS OF VARIATES. *Biometrika* 28, 3-4 (1936), 321–377.
- [15] Harold Hotelling. 1992. Relations between two sets of variates. In *Breakthroughs in statistics: methodology and distribution*. Springer, 162–190.
- [16] Bojian Hou, Andrés Mondragón, Davoud Ataee Tarzanagh, Zhuoping Zhou, Andrew J Saykin, Jason H Moore, Marylyn D Ritchie, Qi Long, and Li Shen. 2024. PFERM: A Fair Empirical Risk Minimization Approach with Prior Knowledge. *AMIA Summits on Translational Science Proceedings* 2024 (2024), 211.

- [17] Leonardo Iaccarino, Gautam Tammewar, Nagehan Ayakta, Suzanne L. Baker, Alexandre Bejanin, Adam L. Boxer, Maria Luisa Gorno-Tempini, Mustafa Janabi, Joel H. Kramer, Andreas Lazaris, Samuel N. Lockhart, Bruce L. Miller, Zachary A. Miller, James P. O'Neil, Rik Ossenkoppele, Howard J. Rosen, Daniel R. Schonhaut, William J. Jagust, and Gil D. Rabinovici. 2018. Local and distant relationships between amyloid, tau and neurodegeneration in Alzheimer's Disease. *NeuroImage: Clinical* 17 (2018), 452–464. <https://doi.org/10.1016/j.nicl.2017.09.016>
- [18] Kei Igarashi. 2022. Entorhinal cortex dysfunction in Alzheimer's disease. *Trends in Neurosciences* 46 (12 2022). <https://doi.org/10.1016/j.tins.2022.11.006>
- [19] Faisal Kamiran and Toon Calders. 2012. Data preprocessing techniques for classification without discrimination. *Knowledge and information systems* 33, 1 (2012), 1–33.
- [20] Michael Kearns, Seth Neel, Aaron Roth, and Zhiwei Steven Wu. 2018. Preventing fairness gerrymandering: Auditing and learning for subgroup fairness. In *International conference on machine learning*. PMLR, 2564–2572.
- [21] Jon Kleinberg, Sendhil Mullainathan, and Manish Raghavan. 2016. Inherent trade-offs in the fair determination of risk scores. *arXiv preprint arXiv:1609.05807* (2016).
- [22] Matthäus Kleindessner, Michele Donini, Chris Russell, and Muhammad Bilal Zafar. 2023. Efficient fair PCA for fair representation learning. In *International Conference on Artificial Intelligence and Statistics*. PMLR, 5250–5270.
- [23] Matt J Kusner, Joshua Loftus, Chris Russell, and Ricardo Silva. 2017. Counterfactual fairness. *Advances in neural information processing systems* 30 (2017).
- [24] Lydia T Liu, Sarah Dean, Esther Rolf, Max Simchowitz, and Moritz Hardt. 2018. Delayed impact of fair machine learning. In *International Conference on Machine Learning*. PMLR, 3150–3158.
- [25] Scott M Lundberg and Su-In Lee. 2017. A unified approach to interpreting model predictions. *Advances in neural information processing systems* 30 (2017).
- [26] Dingailu Ma, Irfete Fetahu, Mei Wang, Rui Fang, Jiahui Li, Hang Liu, Tobin Gramyk, Isabella Iwanicki, Sophie Gu, Winnie Xu, Li Tan, Feizhen Wu, and Yujia Shi. 2020. The fusiform gyrus exhibits an epigenetic signature for Alzheimer's disease. *Clinical Epigenetics* 12 (08 2020). <https://doi.org/10.1186/s13148-020-00916-3>
- [27] David Madras, Elliot Creager, Toniann Pitassi, and Richard Zemel. 2018. Learning adversarially fair and transferable representations. In *International Conference on Machine Learning*. PMLR, 3384–3393.
- [28] EJ Min, EC Chi, and H Zhou. 2020. Tensor canonical correlation analysis. *Stat* 8, 1 (2020), e253. <https://doi.org/10.1002/sta4.253> Epub 2020 Jan 2. PMID: 32655193; PMCID: PMC7351364.
- [29] Nghi Nguyen, Tao Hou, Enrico Amico, Jingyi Zheng, Huajun Huang, Alan D Kaplan, Giovanni Petri, Joaquín Goñi, Ralph Kaufmann, Yize Zhao, et al. 2024. Volume-optimal persistence homological scaffolds of hemodynamic networks covary with MEG theta-alpha aperiodic dynamics. In *International Conference on Medical Image Computing and Computer-Assisted Intervention*. Springer, 519–529.
- [30] Ziad Obermeyer, Brian Powers, Christine Vogeli, and Sendhil Mullainathan. 2019. Dissecting racial bias in an algorithm used to manage the health of populations. *Science* 366, 6464 (2019), 447–453. <https://doi.org/10.1126/science.aax2342> arXiv:https://www.science.org/doi/pdf/10.1126/science.aax2342
- [31] Harold Pimentel, Zhiyue Hu, and Haiyan Huang. 2018. Biclustering by sparse canonical correlation analysis. *Quantitative Biology* 6, 1 (2018), 56–67.
- [32] Changjian Shui, Gezheng Xu, Qi Chen, Jiaqi Li, Charles X Ling, Tal Arbel, Boyu Wang, and Christian Gagné. 2022. On learning fairness and accuracy on multiple subgroups. *Advances in Neural Information Processing Systems* 35 (2022), 34121–34135.
- [33] Ingo Steinwart and Andreas Christmann. 2008. *Support vector machines*. Springer Science & Business Media.
- [34] Davoud Ataee Tarzanagh, Bojian Hou, Boning Tong, Qi Long, and Li Shen. 2023. Fairness-aware class imbalanced learning on multiple subgroups. In *Uncertainty in Artificial Intelligence*. PMLR, 2123–2133.
- [35] M. W. Weiner, D. P. Veitch, P. S. Aisen, et al. 2013. The Alzheimer's Disease Neuroimaging Initiative: a review of papers published since its inception. *Alzheimers Dement* 9, 5 (2013), e111–94.
- [36] Michael W Weiner, Dallas P Veitch, Paul S Aisen, et al. 2017. Recent publications from the Alzheimer's Disease Neuroimaging Initiative: Reviewing progress toward improved AD clinical trials. *Alzheimer's & Dementia* 13, 4 (2017), e1–e85.
- [37] Frederick Xu, Duy Duong-Tran, Yize Zhao, and Li Shen. [n. d.]. Caudal and Thalamic Segregation in White Matter Brain Network Communities in Alzheimer's Disease Population. In *IEEE-EMBS International Conference on Biomedical and Health Informatics*.
- [38] Frederick Xu, Sumita Garai, Duy Duong-Tran, Andrew J Saykin, Yize Zhao, and Li Shen. 2022. Consistency of graph theoretical measurements of Alzheimer's disease fiber density connectomes across multiple parcellation scales. In *2022 IEEE International Conference on Bioinformatics and Biomedicine (BIBM)*. IEEE, 1323–1328.
- [39] Frederick H Xu, Michael Gao, Jiong Chen, Sumita Garai, Duy Anh Duong-Tran, Yize Zhao, and Li Shen. 2024. Topology-based Clustering of Functional Brain Networks in an Alzheimer's Disease Cohort. *AMIA Summits on Translational Science Proceedings* 2024 (2024), 449.
- [40] Huanqing Yang, Hua Xu, Qingfeng Li, Yan Jin, Weixiong Jiang, Jinghua Wang, Yina Wu, Wei Li, Cece Yang, Xia Li, Shifu Xiao, Feng Shi, and Tao Wang. 2019. Study of brain morphology change in Alzheimer's disease and amnesic mild cognitive impairment compared with normal controls. *General Psychiatry* 32 (04 2019), e100005. <https://doi.org/10.1136/gpsych-2018-100005>
- [41] Muhammad Bilal Zafar, Isabel Valera, Manuel Gomez Rogriguez, and Krishna P Gummadi. 2017. Fairness constraints: Mechanisms for fair classification. In *Artificial intelligence and statistics*. PMLR, 962–970.
- [42] Rich Zemel, Yu Wu, Kevin Swersky, Toni Pitassi, and Cynthia Dwork. 2013. Learning fair representations. In *International conference on machine learning*. PMLR, 325–333.
- [43] Daoqiang Zhang, Yaping Wang, Luping Zhou, Hong Yuan, Dinggang Shen, Alzheimer's Disease Neuroimaging Initiative, et al. 2011. Multimodal classification of Alzheimer's disease and mild cognitive impairment. *Neuroimage* 55, 3 (2011), 856–867.
- [44] Yu Zhang, Guoxu Zhou, Jing Jin, Yangsong Zhang, Xingyu Wang, and Andrzej Cichocki. 2017. Sparse Bayesian multiway canonical correlation analysis for EEG pattern recognition. *Neurocomputing* 225 (2017), 103–110.
- [45] Zhuoping Zhou, Davoud Ataee Tarzanagh, Bojian Hou, Boning Tong, Jia Xu, Yanbo Feng, Qi Long, and Li Shen. 2024. Fair Canonical Correlation Analysis. *Advances in Neural Information Processing Systems* 36 (2024).

## A Additional Experimental Results

### A.1 Additional Classifiers

We have conducted additional evaluations using Logistic Regression (LR) classifier shown in Supplemental Table 1 and Multilayer Perceptron (MLP) classifier shown in Supplemental Table 2 as follows. The results confirm that the conclusions drawn from our initial experiments still hold true across distinct classifiers as well. Our FR-CCA shows strong robustness, and it consistently achieves better fairness outcomes while maintaining competitive classification performance across different classifiers and datasets.

### A.2 Additional Fairness Baselines

We have added more baselines in our experiments to validate the effectiveness of the proposed method. Specifically, we have added two more conventional fairness methods: Empirical Risk Minimization under Fairness Constraints (FERM) [10] and its variant: A Fair Empirical Risk Minimization Approach with Prior Knowledge (PFERM) [16]. These two methods tried to do empirical risk minimization for classification tasks under certain fairness constraints (mainly for EO). Note that FERM can significantly improve the fairness performance while sacrificing its accuracy performance. PFERM uses prior knowledge to mitigate this drawback and provides better accuracy performance but a bit inferior fairness performance. The results in Table 1 below show that FERM performs better than PFERM in terms of DPG and EOG while its accuracy is inferior to PFERM which validates our understanding.

At the same time our FR-CCA has a competitive accuracy performance compared with FERM while has the best fairness performance (including DPG, EOG and GSG) compared to FERM and PFERM which demonstrates the effectiveness of our FR-CCA especially in terms of fairness. It is important to note that these conventional fairness methods only focus on fair classification while our method concentrates on both correlation maximization and subsequent fair classification, making the comparison not fair. This is why we didn't include conventional fairness-aware classification methods in our experiment. However, we would like to include these results and discussions in our revised manuscripts to provide a better insight.

### A.3 Detailed Hypothesis Test Results

To validate the performance of the FR-CCA method compared to the CCA method in terms of fairness metrics, we conduct a series of hypothesis testings in this supplemental materials. Specifically, we aim to determine if the fairness metrics (GSG, DPG, EOG) metrics of the FR-CCA method are significantly lower than that of the CCA method. This validation is crucial to ensure that the FR-CCA method offers a substantial improvement in fairness over the traditional CCA method from the statistical perspective, thereby justifying its use in applications where fairness is a critical concern.

Given that our approach involves injecting fairness constraints into the CCA framework, it is logical to use the CCA method as the main baseline for comparison. This allows us to directly measure the impact of the fairness constraints on the performance of the CCA method. We utilize the same samples to perform 50 experiments for both the FR-CCA and CCA methods over 4 modalities. This process generates distributions of three fairness metrics (GSG, DPG, EOG).

To rigorously compare the two methods, we follow these steps:

- First, we conduct the Shapiro-Wilk test on each fairness metric over all modalities to verify the normality of each distribution.
- Based on the result of the Shapiro-Wilk test, we can select the appropriate statistical test.
- If both distributions for FR-CCA and CCA are normally distributed, we use the paired t-test.
- If either distribution deviate from normality, we employ the Wilcoxon signed-rank test, a non-parametric method that does not assume normality.
- Regardless of whether the paired t-test or the Wilcoxon signed test is conducted, we will reject the null hypothesis if the p-value is less than 0.05. This means that the fairness performance of the classifier based on FR-CCA is significantly better than that of the classifier based on traditional CCA.

The results are shown in Supplemental Table 4 and Supplemental Figure 1. From Supplemental Table 4, we can see that among 12 tests, there are 8 Wilcoxon test and 4 Paired t-test. From Supplemental Figure 1 we can see that the distribution of our FR-CCA locates on the left side of that of CCA indicating the superiority of the proposed method.

## B Additional Discussions

### B.1 Group Fairness vs Other Fairness

There are multiple types of fairness measures to consider in machine learning, especially for clinical applications. Our focus on group-based fairness metrics was motivated by their widespread use and interpretability in healthcare contexts. While individual fairness metrics like minimax fairness can offer additional insights, we believe the group-based measures we employed are well-suited for our specific use case of Alzheimer's disease diagnosis for several reasons:

- Interpretability: Group-based metrics are more easily interpretable by clinicians and patients, aligning with how fairness is often conceptualized in healthcare settings (e.g. equal treatment across demographic groups).
- Clinical relevance: In Alzheimer's diagnosis, group-level disparities (e.g. by sex or race) are a major concern, making group fairness metrics directly relevant.
- Data limitations: Individual fairness metrics often require more fine-grained data on individuals' similarity, which can be challenging to define robustly for complex medical data.
- Statistical stability: With limited sample sizes in medical datasets, group-level metrics tend to be more statistically stable than individual-level metrics.
- Alignment with regulations: Many healthcare regulations and guidelines focus on group-level fairness, making our chosen metrics more immediately applicable.

We acknowledge that other fairness metrics could provide complementary insights. In future work, we plan to explore how our FR-CCA method performs on additional fairness criteria, potentially including individual fairness measures like minimax fairness,

**Supplemental Table 1: Comparative fairness and accuracy performance with Logistic Regression Classifier (LR).**

Modality	Metric	LR	CCA	SF-CCA	MF-CCA	FR-CCA
Synthetic X	GSG	$0.320 \pm 0.014$	$0.310 \pm 0.033$	$0.296 \pm 0.043$	$0.303 \pm 0.033$	$0.277 \pm 0.001$
	DPG	$0.230 \pm 0.127$	$0.126 \pm 0.091$	$0.089 \pm 0.067$	$0.085 \pm 0.054$	$0.058 \pm 0.053$
	EOG	$0.148 \pm 0.023$	$0.068 \pm 0.048$	$0.029 \pm 0.021$	$0.029 \pm 0.019$	$0.020 \pm 0.017$
	Accuracy	$0.580 \pm 0.029$	$0.504 \pm 0.019$	$0.535 \pm 0.071$	$0.512 \pm 0.040$	$0.532 \pm 0.019$
Synthetic Y	GSG	$0.302 \pm 0.019$	$0.305 \pm 0.030$	$0.257 \pm 0.027$	$0.276 \pm 0.028$	$0.241 \pm 0.003$
	DPG	$0.277 \pm 0.106$	$0.134 \pm 0.059$	$0.106 \pm 0.048$	$0.108 \pm 0.030$	$0.098 \pm 0.065$
	EOG	$0.033 \pm 0.017$	$0.024 \pm 0.013$	$0.029 \pm 0.018$	$0.029 \pm 0.021$	$0.022 \pm 0.026$
	Accuracy	$0.584 \pm 0.092$	$0.520 \pm 0.028$	$0.531 \pm 0.029$	$0.508 \pm 0.055$	$0.529 \pm 0.026$
ADNI MRI	GSG	$0.332 \pm 0.053$	$0.309 \pm 0.044$	$0.327 \pm 0.051$	$0.297 \pm 0.020$	$0.249 \pm 0.042$
	DPG	$0.077 \pm 0.015$	$0.065 \pm 0.019$	$0.061 \pm 0.041$	$0.061 \pm 0.025$	$0.019 \pm 0.013$
	EOG	$0.108 \pm 0.012$	$0.117 \pm 0.033$	$0.087 \pm 0.022$	$0.078 \pm 0.031$	$0.027 \pm 0.015$
	Accuracy	$0.601 \pm 0.002$	$0.444 \pm 0.036$	$0.513 \pm 0.064$	$0.481 \pm 0.049$	$0.573 \pm 0.031$
ADNI AV1451	GSG	$0.271 \pm 0.059$	$0.297 \pm 0.052$	$0.269 \pm 0.028$	$0.282 \pm 0.058$	$0.266 \pm 0.023$
	DPG	$0.075 \pm 0.065$	$0.064 \pm 0.033$	$0.120 \pm 0.073$	$0.101 \pm 0.028$	$0.041 \pm 0.034$
	EOG	$0.081 \pm 0.033$	$0.058 \pm 0.036$	$0.124 \pm 0.049$	$0.116 \pm 0.024$	$0.049 \pm 0.033$
	Accuracy	$0.636 \pm 0.162$	$0.536 \pm 0.031$	$0.469 \pm 0.103$	$0.506 \pm 0.089$	$0.598 \pm 0.048$

**Supplemental Table 2: Comparative fairness and accuracy performance with Multilayer Perceptron Classifier (MLP).**

Modality	Metric	MLP	CCA	SF-CCA	MF-CCA	FR-CCA
Synthetic X	GSG	$0.274 \pm 0.009$	$0.277 \pm 0.024$	$0.322 \pm 0.033$	$0.315 \pm 0.033$	$0.273 \pm 0.058$
	DPG	$0.553 \pm 0.006$	$0.178 \pm 0.068$	$0.078 \pm 0.059$	$0.074 \pm 0.068$	$0.072 \pm 0.067$
	EOG	$0.306 \pm 0.006$	$0.068 \pm 0.026$	$0.067 \pm 0.030$	$0.046 \pm 0.024$	$0.011 \pm 0.002$
	Accuracy	$0.618 \pm 0.029$	$0.578 \pm 0.025$	$0.568 \pm 0.026$	$0.575 \pm 0.030$	$0.606 \pm 0.006$
Synthetic Y	GSG	$0.306 \pm 0.006$	$0.283 \pm 0.015$	$0.292 \pm 0.019$	$0.298 \pm 0.039$	$0.273 \pm 0.009$
	DPG	$0.553 \pm 0.113$	$0.184 \pm 0.076$	$0.121 \pm 0.042$	$0.118 \pm 0.072$	$0.077 \pm 0.113$
	EOG	$0.112 \pm 0.030$	$0.023 \pm 0.017$	$0.046 \pm 0.019$	$0.036 \pm 0.019$	$0.010 \pm 0.000$
	Accuracy	$0.619 \pm 0.029$	$0.591 \pm 0.018$	$0.587 \pm 0.038$	$0.587 \pm 0.022$	$0.607 \pm 0.012$
ADNI MRI	GSG	$0.284 \pm 0.037$	$0.296 \pm 0.019$	$0.307 \pm 0.011$	$0.307 \pm 0.007$	$0.227 \pm 0.052$
	DPG	$0.078 \pm 0.017$	$0.061 \pm 0.033$	$0.036 \pm 0.013$	$0.034 \pm 0.010$	$0.032 \pm 0.045$
	EOG	$0.067 \pm 0.025$	$0.052 \pm 0.031$	$0.039 \pm 0.020$	$0.032 \pm 0.101$	$0.021 \pm 0.010$
	Accuracy	$0.617 \pm 0.027$	$0.575 \pm 0.036$	$0.602 \pm 0.031$	$0.605 \pm 0.029$	$0.624 \pm 0.019$
ADNI AV1451	GSG	$0.305 \pm 0.071$	$0.317 \pm 0.045$	$0.295 \pm 0.026$	$0.285 \pm 0.059$	$0.277 \pm 0.068$
	DPG	$0.098 \pm 0.059$	$0.088 \pm 0.039$	$0.028 \pm 0.022$	$0.046 \pm 0.044$	$0.031 \pm 0.024$
	EOG	$0.094 \pm 0.030$	$0.067 \pm 0.032$	$0.057 \pm 0.037$	$0.047 \pm 0.035$	$0.035 \pm 0.016$
	Accuracy	$0.646 \pm 0.134$	$0.633 \pm 0.034$	$0.624 \pm 0.015$	$0.621 \pm 0.016$	$0.616 \pm 0.038$

to provide a more comprehensive evaluation of fairness in medical AI systems.

## B.2 Trade-off between Fairness and Accuracy

Our primary objective is to strike the balance between fairness and accuracy performance, recognizing that these two goals are often at odds. The lower accuracy performance observed in FR-CCA as highlighted in Table 1, is largely attributable to the dimensionality reduction inherent in the CCA process applied in the first stage of our method. This process is necessary to identify the shared representation space between two modalities, which inherently leads to a loss of some predictive ability. However, our results

demonstrate that FR-CCA effectively achieves this balance. While the accuracy performance may be slightly lower than others, it still remains so close, and more importantly, FR-CCA consistently outperforms all other methods across all fairness metrics (GSG, DPG, EOG). This shows that FR-CCA achieves its primary goal: ensuring that fairness is improved without sacrificing accuracy too much.

Moreover, an additional strength is that FR-CCA has strongly consistent performance across different modalities, especially in the real data case. This consistency is a direct result of our CCA-based approach, which effectively captures the most correlated representation space between the two modalities, ensuring that the model's

**Supplemental Table 3: Comparative fairness and accuracy performance between FR-CCA and two additional baselines (FERM, PFERM).**

Modality	Metric	FERM	PFERM	FR-CCA
Synthetic X	GSG	$0.500 \pm 0.000$	$0.496 \pm 0.088$	$0.242 \pm 0.046$
	DPG	$0.088 \pm 0.037$	$0.144 \pm 0.087$	$0.026 \pm 0.031$
	EOG	$0.015 \pm 0.015$	$0.022 \pm 0.002$	$0.012 \pm 0.014$
	Accuracy	$0.507 \pm 0.044$	$0.541 \pm 0.017$	$0.492 \pm 0.048$
Synthetic Y	GSG	$0.500 \pm 0.000$	$0.477 \pm 0.101$	$0.216 \pm 0.084$
	DPG	$0.091 \pm 0.059$	$0.071 \pm 0.044$	$0.037 \pm 0.035$
	EOG	$0.024 \pm 0.012$	$0.029 \pm 0.013$	$0.022 \pm 0.010$
	Accuracy	$0.542 \pm 0.039$	$0.595 \pm 0.027$	$0.500 \pm 0.038$
ADNI MRI	GSG	$0.277 \pm 0.011$	$0.342 \pm 0.071$	$0.258 \pm 0.038$
	DPG	$0.071 \pm 0.023$	$0.131 \pm 0.010$	$0.010 \pm 0.011$
	EOG	$0.036 \pm 0.010$	$0.041 \pm 0.045$	$0.014 \pm 0.011$
	Accuracy	$0.593 \pm 0.009$	$0.681 \pm 0.027$	$0.612 \pm 0.037$
ADNI AV1451	GSG	$0.227 \pm 0.052$	$0.329 \pm 0.049$	$0.215 \pm 0.041$
	DPG	$0.080 \pm 0.019$	$0.088 \pm 0.033$	$0.008 \pm 0.006$
	EOG	$0.024 \pm 0.013$	$0.044 \pm 0.080$	$0.010 \pm 0.005$
	Accuracy	$0.633 \pm 0.024$	$0.707 \pm 0.004$	$0.678 \pm 0.013$

**Supplemental Table 4: Results of Shapiro-Wilk test for the fairness metrics (GSG, DPG, EOG) across different modalities (Synthetic X, Synthetic Y, ADNI MRI, and ADNI AV1451) compare the CCA and FR-CCA methods. A p-value less than 0.05 indicates non-normality, leading to the use of the Wilcoxon test. Conversely, p-values greater than 0.05 for both CCA and FR-CCA indicate normality, leading to the use of the Paired t-test.**

Modality		Synthetic X		Synthetic Y		ADNI MRI		ADNI AV1451	
		CCA	FR-CCA	CCA	FR-CCA	CCA	FR-CCA	CCA	FR-CCA
Stats	GSG	0.651	0.955	0.981	0.973	0.938	0.991	0.982	0.975
	DPG	0.958	0.665	0.889	0.931	0.948	0.932	0.860	0.873
	EOG	0.936	0.818	0.989	0.996	0.971	0.987	0.846	0.746
p-value	GSG	$1.193e^{-09}$	$5.241e^{-02}$	$5.898e^{-01}$	$3.100e^{-01}$	$1.107e^{-02}$	$9.660e^{-01}$	$5.713e^{-01}$	$3.522e^{-01}$
	DPG	$7.043e^{-02}$	$2.070e^{-09}$	$2.138e^{-04}$	$6.053e^{-03}$	$2.705e^{-02}$	$6.527e^{-03}$	$2.568e^{-06}$	$7.103e^{-05}$
	EOG	$9.62e^{-03}$	$2.313e^{-06}$	$8.731e^{-01}$	$9.898e^{-01}$	$2.434e^{-02}$	$8.649e^{-02}$	$1.188e^{-06}$	$6.239e^{-08}$
Normality	GSG	No	Yes	Yes	Yes	No	Yes	Yes	Yes
	DPG	Yes	No	No	No	No	No	No	No
	EOG	No	No	Yes	Yes	Yes	Yes	No	No
Type	GSG	Wilcoxon		Paired t-test		Wilcoxon		Paired t-test	
	DPG	Wilcoxon		Wilcoxon		Wilcoxon		Wilcoxon	
	EOG	Wilcoxon		Paired t-test		Paired t-test		Wilcoxon	

behavior is aligned. Unlike other methods, which may perform well on one modality but falter on another, FR-CCA’s consistent performance underscores the effectiveness of our approach in finding a shared representation that generalizes well across diverse datasets. This cross-modal consistency is a unique advantage of our method, further supporting its practical applicability in real-world scenarios where data from multiple sources must be integrated.

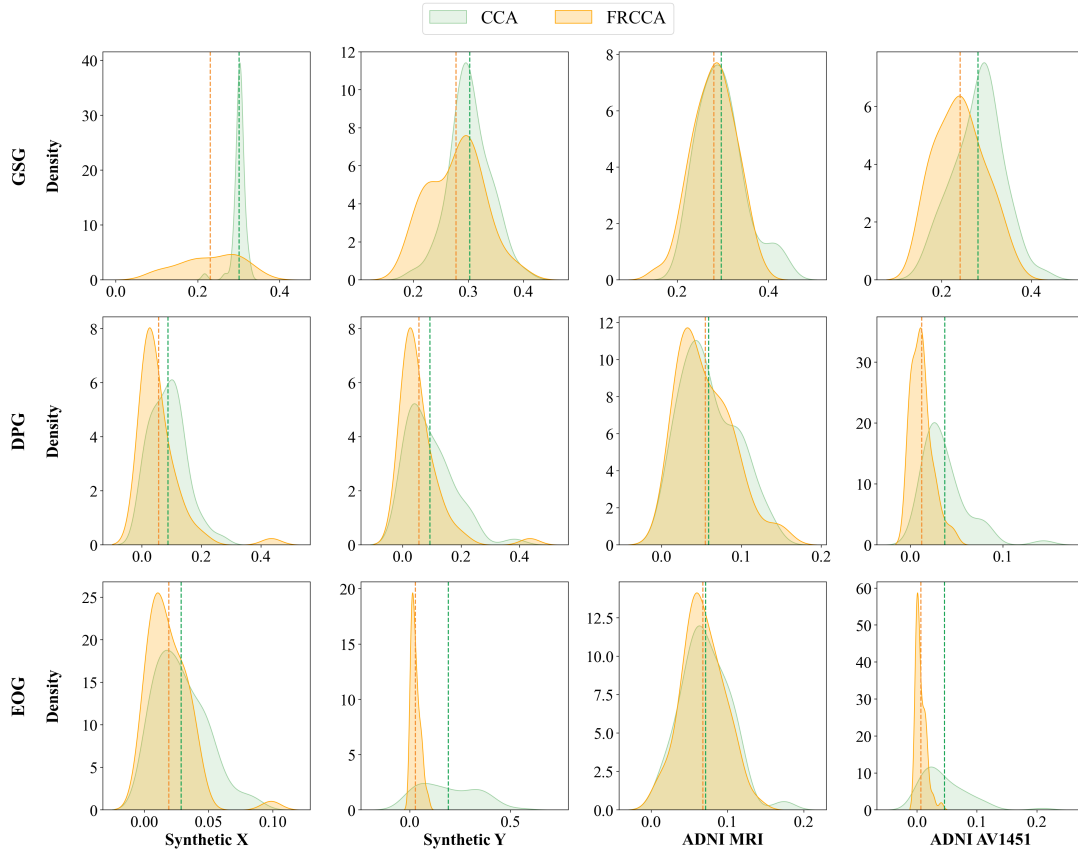
In summary, while the prediction performance of FR-CCA might not be the absolute best in every scenario, this is a balanced trade-off that allows us to achieve superior fairness. The fact that FR-CCA outperforms other methods in all fairness metrics while maintaining competitive accuracy performance highlights the success of our approach in achieving such a balance. Additionally, the consistency across different modalities further strengthens the case

for FR-CCA as a robust and reliable method for application where fairness is a critical concern such as the diagnosis of Alzheimer’s disease. We believe that these results demonstrate that FR-CCA fulfills its primary purpose and offers a valid solution for scenarios requiring a balance between fairness and accuracy across different data modalities.

### B.3 Key Difference between FR-CCA and F-CCA

We will highlight the key differences and design motivations between the proposed Fair Representation CCA (FR-CCA) method and Zhou et al.’s F-CCA approach [45].

*Key Differences:*



**Supplemental Figure 1: Distribution plots of fairness metrics (GSG, DPG, EOG) for CCA and FR-CCA across different modalities (Synthetic X, Synthetic Y, ADNI MRI, ADNI AV1451). The x-axis of each subplot corresponds to the respective fairness metric being evaluated. The dashed lines represent the mean values of these metrics computed over 50 experimental seeds. (The lower, the better)**

- (1) From the objective perspective FR-CCA focuses on learning fair representations that are independent of sensitive attributes, aimed at improving fairness in downstream classification tasks while F-CCA aims to minimize correlation disparity errors associated with protected attributes during the CCA process itself.
- (2) From the perspective of fairness approach, FR-CCA enforces independence between learned representations and sensitive attributes by projecting data onto a nullspace orthogonal to the sensitive attribute while F-CCA introduces fairness constraints directly into the CCA optimization problem to balance correlation across different protected groups.
- (3) In optimization, FR-CCA uses a two-step process - first projecting data to nullspaces, then applying standard CCA, while F-CCA proposes two optimization frameworks (multi-objective and single-objective) that incorporate fairness constraints directly into CCA optimization.
- (4) From the computational complexity perspective, FR-CCA maintains time complexity similar to standard CCA, while

F-CCA introduces additional computational overhead, especially for the multi-objective framework.

- (5) Last but not least, for the downstream task focus FR-CCA explicitly designed to improve fairness in subsequent classification tasks, whereas F-CCA primarily focuses on fairness within the CCA process itself, without specific consideration for downstream tasks.

#### *Design Motivations:*

##### (1) FR-CCA:

- Motivated by the need for fair representation learning that directly translates to fairness in downstream tasks.
- Aims to address limitations of previous fair CCA methods that don't explicitly consider classification performance.
- Designed to be computationally efficient while maintaining fairness and accuracy.

##### (2) F-CCA:

- Motivated by the need to address fairness issues within the CCA process itself.
- Aims to provide a flexible framework for balancing correlation and fairness across different protected groups.



- Designed to offer both automatic (multi-objective) and manual (single-objective) ways to tune fairness-accuracy trade-offs.

In summary, while both methods aim to incorporate fairness into CCA, FR-CCA takes a representation learning approach focused on downstream task performance, while F-CCA focuses on fairness within the CCA process itself. FR-CCA offers a potentially more efficient solution for scenarios where fair classification is the ultimate goal, while F-CCA provides more flexibility in tuning fairness-correlation trade-offs within CCA.

#### B.4 The Choice on $R$

$R$  is the representation dimension that we can choose for the subsequent classification. In our experiments, we followed the same experimental settings as Zhou et al. (2023) [45] in their paper "Fair Canonical Correlation Analysis" to ensure a fair comparison with existing methods. Specifically:

- For synthetic data, we used  $R = 7$  for the unsupervised learning stage to comprehensively evaluate the method's performance across multiple dimensions. However, for the subsequent classification task, we used  $R = 2$  to focus on the most significant canonical correlations and to reduce computational complexity.
- For the ADNI data, we used  $R = 5$ , again following Zhou et al.'s setting. This choice balances between capturing sufficient information from the multimodal data and avoiding overfitting on the relatively smaller real-world dataset.

We acknowledge that the choice of  $R$  can be crucial and may vary depending on the specific dataset and application. In practice, one could determine the optimal through various methods such as:

- Cross-validation to optimize downstream task performance
- Analyzing the decay of canonical correlations
- Using domain knowledge about the expected number of latent factors
- Applying dimensionality estimation techniques

For future work, we plan to conduct a more comprehensive analysis on the impact of different  $R$  values on both representation quality and fairness metrics. This could provide valuable insights for practitioners on how to choose  $R$  for their specific applications.

### C Comprehensive Related Work

Fairness in machine learning has emerged as a critical area of research, addressing the potential for algorithmic bias and discrimination in automated decision-making systems. Seminal work by Dwork et al. (2012) [11] introduced the concept of individual fairness, while Hardt et al. (2016) [13] proposed influential group fairness metrics such as demographic parity and equal opportunity. These foundational studies sparked a proliferation of research into various fairness definitions and their mathematical formulations. Subsequent work has explored the inherent tensions and impossibility results among different fairness criteria [9, 21]. In response to these challenges, researchers have developed a range of mitigation strategies, including pre-processing techniques to modify training data [19], in-processing methods that incorporate fairness

constraints into the learning algorithm [41], and post-processing approaches that adjust model outputs. Recent advancements have focused on causal approaches to fairness [23], intersectional fairness considerations [20], and long-term impacts of fairness interventions [24]. The field has also expanded to address fairness in complex machine learning paradigms, such as fair representation learning [27]. As the societal implications of AI systems become increasingly apparent, interdisciplinary collaborations between computer scientists, ethicists, and domain experts continue to shape the evolving landscape of fair machine learning.

*Canonical Correlation Analysis* CCA, introduced by Hotelling in 1936 [14], has been widely applied across various domains. In the context of representation learning, particularly for cross-modal applications, Deep CCA [3] extended traditional CCA to learn nonlinear transformations of two views of data, enabling the discovery of complex correlations in high-dimensional spaces. This advancement has been particularly relevant in fields such as neuroscience [2] and medicine [44], where multimodal data analysis [29] is crucial. Recent work has also explored probabilistic formulations of CCA [4], further expanding its utility in domains like bioinformatics and computer vision.

*Fairness in Machine Learning* As machine learning models are increasingly deployed in high-stakes decision-making scenarios, ensuring fairness has become a critical concern. Seminal work by Dwork et al. (2012) [11] introduced the concept of individual fairness, while subsequent research has explored various group fairness metrics and their implications [5, 16, 34]. In the context of representation learning, Zemel et al. (2013) [42] proposed methods for learning fair representations independent of protected attributes. This line of research is particularly relevant to our work, as we aim to develop fair CCA methods that mitigate biases while preserving the utility of learned features.

*Fair CCA* Recent efforts have focused on incorporating fairness considerations directly into the CCA framework. Zhou et al. (2024) [45] developed fair CCA methods that minimize correlation disparity errors associated with protected attributes. Their work introduced single-objective fair CCA (SF-CCA) and multi-objective fair CCA (MF-CCA), to ensure equitable correlation levels across different groups. However, these methods primarily focus on the correlation analysis without explicitly considering for downstream tasks. Our work builds upon these foundations, addressing the limitations by jointly optimizing for fairness and classification performance.

*Machine Learning for Alzheimer's Disease (AD)* The application of machine learning to Alzheimer's Disease diagnosis has seen significant advancements in recent years. Multimodal approaches integrating neuroimaging, genetic, and clinical data have enhanced predictive performance [37–39, 43]. In the context of fair machine learning, recent work has highlighted the importance of developing unbiased diagnostic tools that perform equitably across diverse patient groups [30]. Our research contributes to this area by applying fair CCA methods to AD diagnosis, leveraging multimodal data such as PET and MRI imaging information to uncover latent factors that are both critical for accurate diagnosis and unbiased with respect to sensitive attributes.